HYDROLOGIC EXPERIMENTS AND ANALYSIS – THE EFFECT OF MICROTOPOGRAPHY ON RUNOFF GENERATION

A Thesis
Submitted to the Graduate Faculty
of the
North Dakota State University
of Agriculture and Applied Science

By

Daniel Frederick Bogart

In Partial Fulfillment of the Requirements
for the Degree of
MASTER OF SCIENCE

Major Department:
Civil and Environmental Engineering

October 2013

Fargo, North Dakota

North Dakota State University
Graduate School

Title

Hydrologic Experiments and Analysis – The Effect of Microtopography on Runoff Generation

By

Daniel Frederick Bogart

The Supervisory Committee certifies that this ***disquisition*** complies with North Dakota State University's regulations and meets the accepted standards for the degree of

MASTER OF SCIENCE

SUPERVISORY COMMITTEE:

Dr. Xuefeng Chu
Chair

Dr. G. Padmanabhan

Dr. Francis Casey

Dr. Thomas DeSutter

Approved:

4/01/2014
Date

Dr. Dinesh Katti
Department Chair

ABSTRACT

Microtopography is an important factor in hydrologic processes. The purpose of this research was to study the effects of microtopography on runoff generation. Specifically, this was performed through an array of physical experimentation comparing "rough" and "smooth" surfaces under natural and simulated rainfall. Utilizing these types of rainfalls required experimentation to take place in both field and laboratory settings. The range of control factors in this study varied from surface microtopography to soil type, rainfall intensity/pattern, and ambient moisture content. The recorded results of the laboratory study were further compared with the output of a puddle-to-puddle (P2P) overland flow model. The physical experiments showed a trend initially favoring neither the rough nor smooth surface in runoff production. However, in subsequent experiments the rough surface appeared to substantially increase runoff production relative to the smooth surface. Additionally, good agreement was found between the results of the physical experimentation and the model.

ACKNOWLEDGMENTS

Firstly, I would like to extend huge gratitude to my advisor, Dr. Xuefeng Chu, who encouraged me since before I started my graduate studies. Dr. Chu secured a place and funding for me to make my graduate studies possible. Additionally, Dr. Chu provided a great deal of guidance and support in my graduate career.

I should also like to extend my thanks to my committee members for their contributions to my research. Dr. Frank Casey, and Dr. Thomas DeSutter provided great insight early on in my research, particularly concerning some very technical matters and instrumentation. Dr. G. Padmanabhan provided many helpful comments and suggestions in paper writing efforts as well as being incredibly supportful. I also am grateful to Dr. Lyle Prunty and Joel Bell of the Soil Science Department for their technical assistance and the use of their laboratory facilities.

I also owe much gratitude to my research colleagues whose combined efforts made my research efforts possible. Specifically, many thanks to Leif Sande, Yaping Chi, Yang Liu, Yingjie Yang, Tyler Brown, and Shravan Avadhuta. In particular, I would like to thank Jun Yang for his unparalleled technical help, support and friendship.

Finally, my sincerest thanks belong to my family. Their love and support allowed me to continue pursuing studies in both my undergraduate and graduate careers. This material is based upon work supported by the National Science Foundation under Grant No. EAR-0907588. Without this financial support, none of this research would have been possible. Any opinions, findings, and conclusions or recommendations expressed in this material are those of the author and do not necessarily reflect the views of the National Science Foundation.

TABLE OF CONTENTS

ABSTRACT iii

ACKNOWLEDGMENTS iv

LIST OF TABLES viii

LIST OF FIGURES ix

LIST OF SYMBOLS xi

CHAPTER 1. INTRODUCTION 1

1.1. Hydrologic Connectivity 3

1.2. Runoff Generation 5

1.3. Objectives 7

CHAPTER 2. EFFECT OF MICROTOPOGRAPHY ON OVERLAND FLOW GENERATION UNDER NATURAL RAINFALL 10

2.1. Abstract 10

2.2. Methods and Materials 10

2.2.1. General Methodology 10

2.2.2. Description of Field Plots 11

2.2.3. Field Data Collection 12

2.2.3.1. Acquisition of Surface DEM Data 12

2.2.3.2. Soil Moisture Data 13

2.2.3.3. Tipping Bucket Rain Gauge 14

2.2.3.4. Outlet Flow Collection 14

2.2.4. Surface Microtopography and Delineation 15

2.2.4.1. Introduction to the PD Program 15

2.2.4.2. Contributing Areas for Puddles and Sub-basins 16
2.2.4.3. Mass Balance Analysis 17
2.3. Results and Analysis 17
2.3.1. Puddle Delineation 17
2.3.2. Soil Moisture 19
2.3.3. Hyetographs and Hydrographs 21
2.3.4. Puddle Connectivity 23
2.3.5. Mass Balance Analysis 26
2.4. Summary and Conclusions 28
CHAPTER 3. LABORATORY OVERLAND FLOW EXPERIMENTS AND MODELING 31
3.1. Introduction…….. 31
3.2. Methods and Materials 31
3.2.1. Laboratory Materials and Equipment 31
3.2.1.1. Soils and Soil Processing 32
3.2.1.2. Soil Box and Soil Packing 33
3.2.1.3. Rainfall Simulator 36
3.2.2. Laboratory Experiments 36
3.2.3. Model Simulations Using P2P Software 39
3.2.3.1. Introduction to the P2P System 39
3.2.3.2. Determination of Soil Hydraulic Parameters 41
3.2.3.3. Comparison of Experiments and Model Simulations 42
3.3. Results and Analysis 44
3.3.1. Laboratory Physical Experiments 44

3.3.1.1. Soil Type Effects....44
3.3.1.2. Rainfall Effects – Steady Rainfall....48
3.3.1.3. Rainfall Effects – Unsteady Rainfall....50
3.3.1.4. Rainfall Effects - Complex Rainfall Series....52
3.3.1.5. Initial Soil Moisture Effects....55
3.3.2. P2P Modeling....56
3.3.2.1. Complex Rainfall Series Comparisons....56
3.3.2.2. Soil Type Comparisons....58
3.3.2.3. Initial Soil Moisture Conditions....61
3.3.3. Other Laboratory Surface....65
3.4. Summary and Conclusions....66
CHAPTER 4. CONCLUSIONS AND FUTURE RESEARCH....68
LITERATURE CITED....71

LIST OF TABLES

Table		Page
2.1.	Individual and Combined Puddle Contributing Areas	19
2.2.	Contributing Areas of Combined or Connected Depressions	24
2.3.	Mass Balance Estimation for the Field Experiments	27
3.1.	Physical Laboratory Experiments	37
3.2.	Physical Experiments Selected to Compare with Simulated Results from P2P Model	43
3.3.	Normalized Objective Function (NOF) and Modeling Efficiency (EF) Values of the Observed and Simulated Discharges for Event 1 of Experiment 1	57
3.4.	Normalized Objective Function (NOF) and Modeling Efficiency (EF) Values of the Observed and Simulated Discharges for Experiments 2 and 3	59
3.5.	Normalized Objective Function (NOF) and Modeling Efficiency (EF) of the Observed and Simulated Average Wetting Front Depths for Experiments 2 and 3	61
3.6.	Normalized Objective Function (NOF) and Modeling Efficiency (EF) of the Observed and Simulated Discharges for Experiments 4-6	63
3.7.	Normalized Objective Function (NOF) and Modeling Efficiency (EF) of the Observed and Simulated Average Wetting Front Depths for Experiments 4-6	64
3.8.	Normalized Objective Function (NOF) and Modeling Efficiency (EF) of the Observed and Simulated Average Wetting Front Depths for Experiment 7	66

LIST OF FIGURES

Figure		Page
1.1.	Puddle to Puddle Processes	2
2.1.	Soil moisture sensor locations and relative depths from the soil surface used on the rough and smooth surfaces.	14
2.2.	DEMs of the rough and smooth surfaces.	18
2.3.	Volumetric water content readings from the soil moisture sensors during each rain event	20
2.4.	Hyetograph and hydrographs for the rough and smooth surfaces for rain event 6/26/2011	22
2.5.	Hyetograph and hydrographs for the rough and smooth surfaces for rain event 8/12/2011	22
2.6.	Contributing area increases of the rough surface versus cumulative rainfall for two events	24
2.7.	Cumulative outlet flow versus cumulative rainfall for the rough and smooth surfaces for rain events 6/26/2011 and 8/12/2011	25
3.1.	DEMs of topographic surfaces	44
3.2.	Comparison of the rough and smooth surface hydrographs for three soils (Experiments A, B, and C for silty clay loam, loamy sand, and silty clay soils, respectively)	45
3.3.	Comparison of the rough and smooth surface hydrographs under 3.54 cm/hr rainfall (Experiment D) and 5.95 cm/hr rainfall (Experiment E) using a silty clay soil	48
3.4	Comparison of the rough and smooth surface hydrographs for an unsteady rainfall pattern. Rainfall intensities in chronological order were 5.95 cm/hr, 1.16 cm/hr, 3.54 cm/hr, and 5.95 cm/hr for 25.0, 42.5, 16.5, and 8.0 minutes, respectively	50
3.5.	Complex rainfall event 1: rough and smooth surface hydrographs using a silty clay soil	52

3.6. Complex rainfall event 2: rough and smooth surface hydrographs using a silty clay soil. (Note that time axis is relative to the beginning of the first rainfall event).....53

3.7. Complex rainfall event 3: rough and smooth surface hydrographs using a silty clay soil. (Note that time axis is relative to the beginning of the first rainfall event).....53

3.8. Rough and smooth surface hydrographs of Experiments H, I, and J using initial moisture contents of 0.207, 0.165, 0.12 cm^3/cm^3, respectively.....55

3.9. Comparison of the observed and simulated hydrographs for Experiment 1 during a complex rainfall series on silty clay 57

3.10. Comparison of the observed and simulated ponding and spilling times for rain event 1 of Experiment 1 using a silty clay soil. 58

3.11. Comparison of the observed and simulated hydrographs for Experiments 2 and 3, using a silty clay loam and loamy sand, respectively 59

3.12. Comparison of the observed and simulated ponding times spilling times for Experiments 2 and 3 using a silty clay loam and loamy sand, respectively 60

3.13. Comparison of the simulated and observed average wetting front depths for Experiments 2 and 3, using a silty clay loam and loamy sand, respectively 61

3.14. Comparison of the observed and simulated hydrographs for Experiments 4-6, using a silty clay soil and comparing initial moisture contents of 0.207, 0.165, 0.12 cm^3/cm^3, respectively.....62

3.15. Comparison of the observed and simulated ponding times spilling times for Experiments 4, 5, and 6, using a silty clay soil and comparing initial moisture contents of 0.207, 0.165, 0.12 cm^3/cm^3, respectively 64

3.16. Comparison of the simulated and observed average wetting front depths for Experiments 4 – 6, using a silty clay soil and comparing initial moisture contents of 0.207, 0.165, 0.12 cm^3/cm^3, respectively 64

3.17. Comparison of the observed and simulated hydrographs for Experiment 7, using a silty clay loam.....65

3.18. Comparison of the simulated and observed critical times of puddle filling and spilling processes for Experiment 7 using a silty clay loam 65

3.19. Comparison of the simulated and observed average wetting front depths for Experiment 7 using a silty clay loam 66

LIST OF SYMBOLS

I .....Incremental infiltration

P .....Incremental rainfall

PD .....Puddle Delineation (program)

Q.....Measured runoff

RP.....Rough Plot

SP .....Smooth Plot

ΔS.....Depressional storage change

n.....Total number of data points

o..... Denotes observed data

P2P .....Puddle-to-Puddle (program)

s.....Denotes simulated data

X .....State variable

$\bar{X}$.....Mean of state variable

CHAPTER 1. INTRODUCTION

Microtopography is recognized as one of the important parameters of the hydrologic response of a soil surface to rainfall (Hairsine et al. 1992; Govers et al. 2000). Microtopography or roughness is typically associated with changes or irregularities on the surface. Surface roughness has been categorized in different ways depending on relative scale and formation (e.g., soil clods and oriented roughness) (Römkens and Wang 1986). Surface roughness, caused by natural forces or external ones such as tillage, gives rise to surface depression storage (Johnson et al. 1979; Onstad 1984). Depression storage over a field is a parameter of special interest because of its perceived ability to capture water and suspended soil particles before they exit to an outlet. It is for this reason that the effects of microtopography with respect to runoff generation and erosional studies on soil surfaces are typically researched simultaneously. However, this study focuses on runoff generation, potential retention, and properties of puddle connectivity.

Chu (2011) described surface roughness effect on runoff generation in four conceptual stages. The first stage is one that is dominated by infiltration. During this time all rain water impacts the surface will infiltrate into the soil. When the rain intensity exceeds the infiltration capacity, excess rainfall will be produced on the surface. This phenomenon marks the end of the first stage and leads into the second one, referred to as the "puddle to puddle" (P2P) filling-spilling-merging process. It is the time period wherein water on the surface begins to fill depressions and eventually exceeds the maximum depression storage (MDS), and flows downstream. During this process puddle relationships, such as combination, are realized. During this phase, runoff will begin to flow to the outlet. To expand on this process, after ponding has begun within puddles they individually begin to

fill. Given enough ponded water, the water level within a puddle begins to rise to its threshold level. At that level the puddle begins to spill in the downstream direction. When a puddle is in the spilling phase, the local area that is draining to the depression is now indirectly flowing downstream, via the puddle, although not necessarily to the outlet. In some cases, two puddles will share a common threshold. In such a case, once the water level of both puddles has reached the common threshold level, they are in a combined relationship forming an overall larger puddle. The water level will rise and fall for the combined puddle simultaneously, so long as it is higher than the common threshold. The combined puddle's water level will rise until it meets the spilling threshold and all local contributing areas to the puddle will now be contributing to the downstream direction. The P2P process is completed once all depressions over the surface have been fully filled, including puddles in a combined relationship. The end of this stage is marked by full surface connectivity to an outlet. Fig 1.1 displays the P2P process wherein puddles begin ponding, filling, merging, and finally reach a fully connected state.

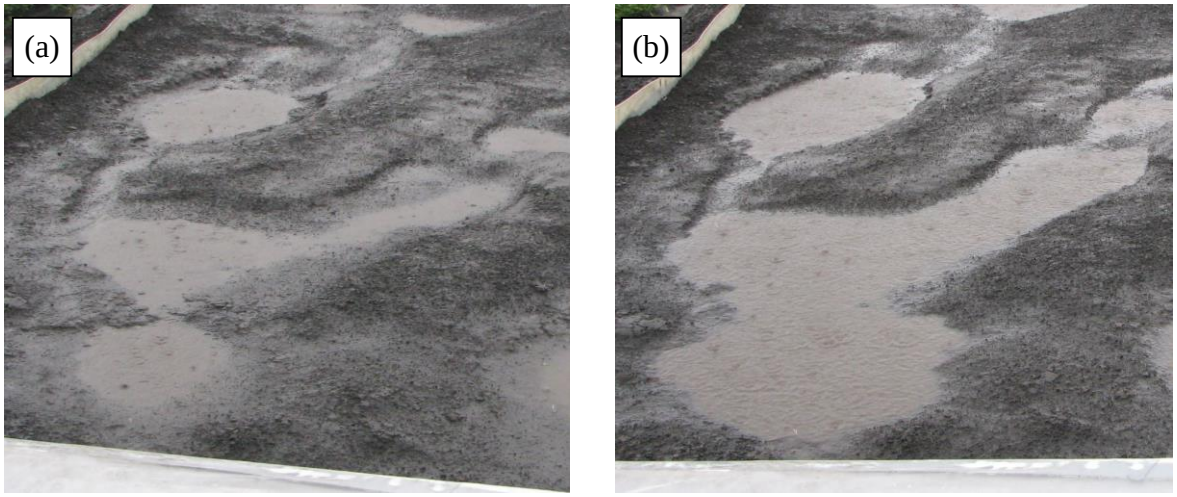

Figure 1.1. Puddle to Puddle Processes (a) Puddles in the filling and spilling phases of the P2P process. (b) Fully filled condition with puddle combination relationships achieved.

The “transition” phase follows and is a time when the surface is fully connected however the flow rate is not yet at a steady state. During this time the infiltration capacity rate is continuing to descend thus increasing the rate of runoff at an outlet, assuming a steady state rainfall. The infiltrability of soil will continue to decrease until it has asymptotically leveled to its final infiltration capacity. Once the infiltrability has reached that point, the flow at the outlet should maintain a constant rate and hence the steady-state stage has been reached.

1.1. Hydrologic Connectivity

Surface depression storage is often treated as an abstraction, wherein its volume should be subtracted from total rainfall before surface runoff is considered possible. However, several experimental studies have concluded that surface runoff will begin before the excess rainfall fills the MDS volume (Moore and Larson 1979; Onstad 1984; Darboux et al. 2001). Therefore more excess rainfall would be required than the MDS to achieve full connectivity to the outlet. Moore and Larson (1979) considered these concepts of depression filling and its effect on contributing area. They noted that at any given time the ratio of collected runoff volume to its cumulative maximum must be less than or equal to the ratio of surface storage to the MDS. Moore and Larson (1979) concluded that contributing area increases were of a stepwise fashion over the course of a rainfall event. That is, the contributing area of a surface increased by instantaneous jumps when the water level of an upstream puddle met its threshold and overflowed in the downstream direction. At such a time, the locally draining area that was previously filling the depression then began contributing runoff to the outlet (assuming that all of its relevant downstream depressions had been fully filled). Darboux et al. (2001) used a numerical model based on the condition

walker method (Chase 1992; Favis-Mortlock 1998) which modeled filling depressions based on the consecutive DEMs taken from the same surface following physical rain from a rainfall simulator. The surface was scanned digitally between rain events and used for the model simulation. The results of the simulation showed that the runoff coefficient of a surface, plotted against the rain volume input, increased faster for subsequent rain events. For the initial surface, a rain input volume that was equivalent to the depression storage was a saddle point where the runoff coefficient showed rapid acceleration in between two periods of slow change. However for subsequent events the runoff coefficient had risen more steadily from the beginning to end of the simulation. This steadying effect increased with further rain events. The authors posited that the homogeneity of the puddles allowed for the uniform connectivity characteristics and thus sharp increase in runoff generation for the original surface. For subsequent events, after erosional and depositional effects had taken place, the connectivity of overland flow, and thus runoff, was more sensitive during initial rain input and less so after an amount of rain equivalent to the storage capacity. The authors reasoned that the increased connectivity was caused by erosional forces that progressively better connected puddles in subsequent rainfalls.

As puddles reach their overflow thresholds and begin connecting to one another, the average connectivity length over the surface will increase, which is a phenomenon described by Darboux et al. (2002). The connectivity length is the average flow length of areas that have become hydrologically connected across the surface yet are not contributing to the outlet. During this process, mass redistribution of soil particles begins. As Darboux et al. (2002) noted, these processes may alter the properties of a surface before runoff even

begins. Over the course of a rain event the connectivity length rises and falls as puddles reach their threshold but then eventually connect to the outlet.

Effects of DEM resolution on surface depression properties and hydrologic connectivity were considered by Yang and Chu (2013a). To convey the effects of DEM grid size on hydrologic connectivity two dimensionless parameters were introduced: the DEM representation scale, the ratio of the DEM grid size to correlation length, and the surface roughness scale, the ratio of random roughness to correlation length. It was generally found that DEMs of a coarser resolution, causing a higher DEM representation scale, markedly influenced perceived hydrologic connectivity. This was found to be particularly true at the early stages of the rainfall-runoff processes.

Additionally, recent advancements in hydrologic connectivity have been made by Yang and Chu (2013b). A puddle-to-puddle model (Chu et al. 2013) was used to quantify the spatio-temporal dynamics of hydrologic connectivity. Various factors such as surface topography, rainfall, and surface slope, were evaluated on their effects on hydrologic connectivity. These factors were shown to significantly affect hydrologic connectivity. For example, the results of the study showed that critical slopes could exist wherein a sharp change in the flow drainage area and hydrologic connectivity was observed.

1.2. Runoff Generation

Regarding runoff generation, varying conclusions have been reached as the result of experimental studies over the last several decades. Some studies have suggested that rough surfaces will have lower total runoff output (Johnson et al. 1979; Cogo et al. 1984). The initial thought that rough surfaces will necessarily contribute less runoff to the outlet than smooth surfaces may be intuitive. Indeed, the NRCS curve number method used in

watershed scale modeling, considers depression storage to be an initial abstraction from excess rainfall before surface runoff may occur (USDA, 1986). Additionally, one may consider the increased ponded area that comes with higher levels of depression storage could influence infiltration by way of increasing areal ponding head over the surface. However, other studies of similar focuses have found that surface roughness did not have a statistically significant effect on overall runoff generation (Helming et al 1998; Darboux and Huang 2005; Gomez and Nearing 2005).

Helming et al. (1998) examined multiple rain events for several levels of surface roughness at steep, moderate, and gentle slopes. The results of the study showed that for the first rain event the medium and rough surfaces contributed a higher final flow rate. However, considering the runoff volume for all subsequent events the roughness levels did not have a significant effect on total runoff generation. Gomez and Nearing (2005) had differing results from a set of experiments also comparing multiple slopes in conjunction with rough versus smooth surface conditions. They reported that on a moderate slope the smooth surface generated more runoff for the first trial; however the rough surface had higher terminal runoff rates in all subsequent rain events. The increased runoff generation from the rough surface of subsequent rainfalls was attributed to sediment deposition in depressions and therefore lowered infiltration. This overall effect negated any significance that microtopography had on runoff generation when considering all experiments. It is important to note the distinction that the runoff generational characteristics of the surfaces changed with subsequent rain events thus not allowing the authors to make any statistical inferences of the effects of surface roughness.

Darboux and Huang (2005) conducted a similar study but discussed more possible scenarios that could affect outflow. These additional inputs included run-on from a feeder box and the occurrence of drainage and seepage phases in the subsurface. The authors found a significant effect of initial depressions on runoff generation. Rough surfaces were contributing up to 10% higher steady-state flow for most experiments. They noted that the differences in their studies to past ones likely lie in the experimental setups. They ultimately determined that results on the general effects of roughness on runoff generation are not conclusive. In short, there is no clear consensus on how rougher surfaces affect runoff generation.

1.3. Objectives

The aforementioned studies used controlled rainfall simulations, mainly in laboratory scale settings, to compare overland flow phenomena and runoff generation between rough and smooth surfaces. The objective of this study was to further look into the development of runoff generation while considering surface microtopography in both laboratory and field conditions. In both methods of experimentation, two types of surfaces (rough and smooth surfaces) were considered to better understand the effects of microtopography. The rough surface was populated with mounds and depressions to give rise to surface depression storage and non-sheet flow hydraulics. The smooth surface was essentially a plane inclined to the same slope of its rough surface counterpart. During experimentation, the surfaces were scanned with a high resolution laser scanner to extract the relative microtopographic changes in their surfaces. Extracting such information was required to calculate the storage volume caused by surface depressions. Additionally, runoff was collected from both surfaces, along with rainfall input, wetting front data (for the

laboratory experiments), and soil moisture data. The combined use of these data alone allowed for a detailed comparison of the effects of microtopography on runoff generation and the analysis of water mass balance over the entire system.

Chapter 2 of this thesis considers the field study conducted under this research, which utilized natural rainfall to produce runoff over two field plots. Two rainfall events during the summer of 2011 were intercepted and of high enough intensity and duration to allow for the production and capture of runoff from both surfaces. Additionally, visual observation and photographic evidence of rough surface depressions filling and overflowing during the rain events were captured. A windows-based Puddle Delineation (PD) software package developed by the Overland Flow Laboratory (Chu et al. 2010a), was used to compute the storage volume and contributing areas of the rough surface. The puddle threshold-controlled spilling times of depressions and their respective contributing area increases were compared to the hydrographs of the rough and smooth surfaces to better understand the role of surface microtopography in runoff production.

Chapter 3 of this thesis considers the laboratory study, which used a more controlled setting within the Overland Flow Laboratory. A rough surface mold (Sande et al. 2011) was utilized to replicate surfaces that were used in an array of experiments to compare additional factors of hydrology in conjunction with microtopography. The hydrologic factors considered were soil type, rainfall intensity and patterns, and initial moisture content. Similar to the field study, the topographic information of each surface was collected along with runoff and soil moisture information. The experiments were then simulated using a Windows-based P2P modeling software package (Chu et al. 2013). The results of the P2P model were compared with the observed data from the physical experiments. This software

is able to delineate surfaces and model the puddle filling, spilling, merging, and splitting processes on impervious and infiltrating topographic surfaces under various soil and rainfall conditions.

CHAPTER 2. EFFECT OF SURFACE MICROTOPOGRAPHY ON OVERLAND FLOW GENERATION UNDER NATURAL RAINFALL

2.1. Abstract

The objective of this study was to examine the effect of microtopography variation on overland flow generation under natural rainfall. Two field plots were used for the observation and collection of runoff under natural rainfall. One surface was shaped to have distinct mounds and depressions giving rise to puddle connectivity while the other had little variation. High resolution DEM data were extracted and surface microtopographic features were analyzed using a puddle delineation (PD) software package. Rough surface puddle connectivity was observed and related to other measured data, such as rainfall and outlet flow. Water mass balance analysis was performed for both surfaces based on the observed rainfall and runoff data as well as the computed depression storage. The data showed that the smooth surface hydrograph was more responsive to the hyetograph particularly for the first rain event. However, during the second rainfall event, the rough surface required less rainfall input to achieve surface connectivity. The "quicker" puddle connectivity for the second rain, given lower rain input volumes, on the rough surface was caused by a change in its apparent infiltrability. This lower apparent infiltrability of the rough surface allowed it to contribute a nearly equivalent volume of runoff to the smooth surface, notwithstanding its considerably higher depressional storage.

2.2. Methods and Materials

2.2.1. General Methodology

The objective of this study was to analyze the role of microtopography by comparing runoff generation under natural rainfall events in the field between a rough soil surface,

consisting of mounds and depressions, and a smooth soil surface. To execute such a study, two naturally occurring rain events were intercepted and puddle connectivity was observed. Additionally, puddle connectivity was quantified, in part, using the Windows-based PD software (Chu et al. 2010a), which was able to discern surface microtopographic features such as puddles and their hierarchical relationships using DEM data. Combined with the observational threshold overflow on the rough surface plot, characterization of the hydrograph was described based on these threshold surface events and depression storage effect. Rain input, depression storage, and the outlet flow data were collected to provide the necessary components for a basic mass balance analysis of the experiments.

2.2.2. Description of Field Plots

Two field plots were selected and set up at the Main Station of the North Dakota Agricultural Experiment Station (NDAES) at NDSU in Fargo, ND (43˚53’33.95” N, 96˚48’52.08” W). Each plot was 6.0 m by 3.5 m. The overland flow from each plot led to an outlet which was located on the outside edge of the field boundary. The soil, on which these plots were constructed, is listed as Fargo (fine, smectitic, frigid Typic Epiaquerts) silty clay. Hydrometer testing of the soil showed that it was a silty clay with 17.5% and 82.5% silt and clay, respectively. Both plot surfaces were graded to have an approximate slope of 2.5% towards the outlet. Construction of the plots started in mid May 2011 and took approximately one month to complete. The first step in construction was to set the borders of the plots in place. The border walls of the plots were 25 cm wide and 1 cm thick plastic sheets. The border walls were pounded into the soil to a depth of 10 - 15 cm. Then, a sheet metal outlet was created and installed for each field plot, which was connected to a water

collection device that was made from a piece of rain gutter and a set of PVC pipes. The entire outlet structure was covered by a large plastic sheet to exclude rain.

The main difference between the plots was their topographic conditions. The first plot's surface (hereupon referred to as the rough plot or RP) was formed with small hand tools to have many surface depressions and mounds with various puddle to puddle relationships and several mini-basins. The second plot (hereupon referred to as the smooth plot or SP) was an essentially inclined plane that had a naturally small degree of surface roughness (e.g., 1 – 5 cm soil aggregates). Each plot led surface runoff to the outlet where water was collected and recorded. Also, installed in the subsurface of each plot, were a number of soil moisture sensors (Decagon ECH2O EC-5). Upon completion of the field plots and their surfaces, the plot areas were covered with large impermeable tarps to protect them from external forces when the plots were not directly supervised.

2.2.3 Field Data Collection

2.2.3.1. Acquisition of Surface DEM Data

To characterize surface microtopography of the runoff plots, the surfaces were first scanned with an instantaneous-profile laser scanner (Huang and Bradford 1990; Darboux and Huang 2003) to obtain the DEM data. Due to the size of the plots and the scanning swath of the laser scanner, a system had to be created to scan each plot in sections to extract all possible surface data. This was done by setting up a rail system that allowed the scanner to rest evenly while taking scans across the surface and maintaining the same relative height above the surface. Once a section of the plot was scanned, the laser scanner was slid down the rail to obtain the next "strip" of DEM data. Scans were taken in such a way as to allow for an overlap (approximately 10 cm) of the scanned areas. Overlapping was ensured by

placing easily identifiable small wooden blocks at 10 cm intervals which were picked up by the laser scanner, similar to a process referred to as "benchmarking" by Darboux et al. (2001).

Overlapping scans served two purposes: the first was the assurance that all DEM data were extracted and the second was that the similar DEM data were recognizable and could be used to create a larger digital surface from two scans. Once two overlapping scans were taken they were combined into a single scan using a software tool, developed in this research project (Chu et al. 2011). Consecutive scans were added to the surface DEM data until the entire plot surface was completed.

2.2.3.2. Soil Moisture Data

Decagon EC-5 Soil moisture sensors were installed in the subsurface of both plots. Fig. 2.1 displays the locations and depths below the surface, at which the sensors were installed. Once set into place the sensors were programmed to take moisture measurements at one minute intervals. The moisture readings continued virtually throughout the duration of the experiments (i.e., moisture readings were logged between, during, and after rainfall events). Such a vast record of real time data allowed for the estimating of initial moisture content before rainfall events and the changes in moisture content at various locations over both plots.

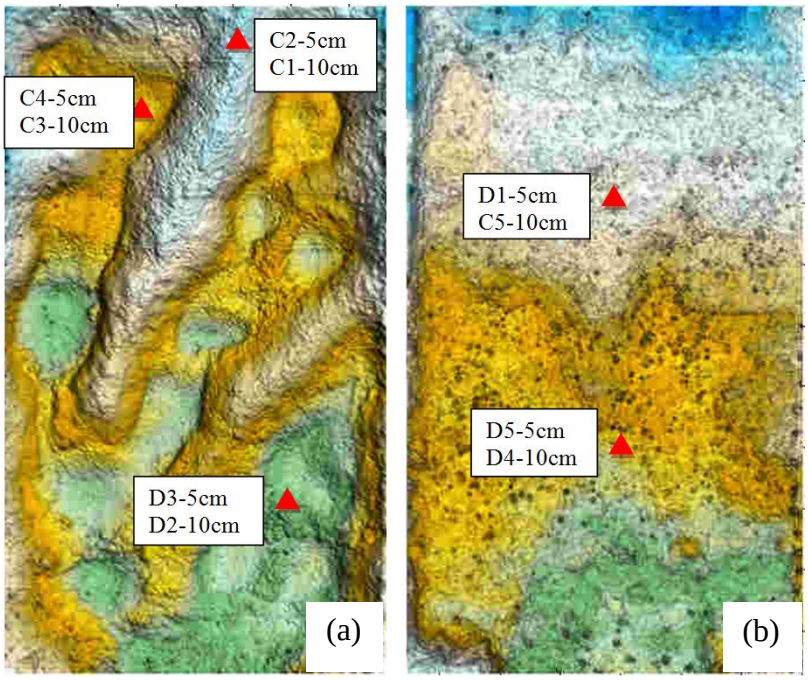

Figure 2.1. Soil moisture sensor locations at depths of 5 and 10 cm for both rough and smooth surfaces. (a) Rough surface. (b) Smooth surface.

2.2.3.3. Tipping Bucket Rain Gauge

The field study involved in this research employed a tipping bucket rain gauge (HOBO data logging rain gauge – RG3) to measure the naturally occurring rain events. The recorded rainfall data were processed and both cumulative and incremental rain data were generated. Raw data output from the tipping bucket rain gage came in the form of a data spread of the exact time that, a volume of 0.01 inches over the gage's catch area, was collected in the gage. From this volume increment and recorded differences in time, the total cumulative rainfall and the hyetograph of a storm were calculated.

2.2.3.4. Outlet Flow Collection

After all preparations had been complete, the field plots were left until a natural rainfall event occurred. The large tarps that covered the plots were then removed from the

surface. Once ponding and subsequent incipient runoff occurred and made its way to the outlet, the runoff was collected by graduated cylinders. Surface runoff at the outlet was collected and measured at a constant time interval of one minute. The flow data were then used to construct the outlet hydrographs. Additionally, photographs were taken to record the P2P process related events occurring on the plots, which included surface ponding, depression filling, and in some cases, puddle combination to higher level puddles. The time electronic stamps of the pictures were used to analyze the temporal connectivity of the rough surface since each puddle has a certain amount of drainage area leading flow to it. These data were used later to compare the contributing area associated with these depressions to the discharge curves of the rough surface and also surface connectivity differences between events.

2.2.4. Surface Microtopography and Delineation

2.2.4.1. Introduction to the PD Program

The scanned DEM data of the RP and SP were loaded into the PD software (Chu et al. 2010a). The PD software has the ability to delineate puddles, flow directions and accumulations, and puddle combination relationships based on the DEM. The algorithm to identify and delineate puddles starts by finding cells that are at an equivalent or lower elevation than its eight neighboring cells. Such a cell is then labeled as a puddle center. A reiterative process then begins and seeks out the lowest cell adjacent to the puddle cell and adds it to a puddle cell sorting list. Threshold cells are identified when an adjacent cell to the latest added puddle cell is found to be of a lower elevation than the puddle cell. Physically, this corresponds to the water level in the puddle rising to a point of overflow and water is able to spill out of the puddle and flow downstream. In some instances, puddles may share a

threshold and therefore one will spill into the other until the free surfaces of both puddles are at an equivalent elevation. Once both puddles have risen to the common threshold elevation, they create an altogether new puddle of a higher level. The combined puddle will continue to fill until the next highest threshold point is met by the free surface. Higher level puddles can also be referred to as in a combined status. The PD program will use the input DEM to delineate puddles and identify their relationships to other puddles until all thresholds have been achieved and the surface is in a fully filled condition.

The PD program also calculates the MDS and the maximum ponding area (MPA) over the entire surface. The depression storage is calculated by the relative elevation differences between puddle cells and their respective threshold cells corresponding to the fully filled status. The MPA of a puddle is the sum of the areas of all puddle cells. The resolution of the DEM data used for the PD program should be carefully considered because varying resolutions have a definite effect on the calculated MDS and MPA of a given surface (Chu et al. 2010b). The resolution of the DEM data used in this field study was 2 cm.

2.2.4.2. Contributing Areas for Puddles and Sub-basins

The PD program also determines flow directions, flow accumulations, and contributing areas for any given points/cells based on the D8 method (O'Callaghan and Mark, 1984). The contributing area for a point/cell can be given either for a fully filled or unfilled condition in the puddle delineation. In the fully filled condition, if a puddle cell is selected, all cells in the puddle, including their own contributing areas plus any contributing areas of any upstream puddles, will be added to the total contributing area. The entire puddle will be included in this area because water in a filled puddle can be from any area

that originally contributes to filling the depression. In the unfilled condition, selecting a puddle center cell will find the area that contributes only directly to that specific cell. It will not consider the upstream puddles and their contributing areas since those depressions have not been fully filled. Both of these conditions have been used in finding the contributing areas of individual puddles and sub-basins for the rough surface.

2.2.4.3. Mass Balance Analysis

Using the measured rainfall, outlet flow data, and the MDS from the PD software, a basic mass balance of the system can be calculated. The final results represent the partition of the rainfall volume at the end of the event. The water mass balance for the plot surface for any time period can be expressed as:

$$\Delta S = P - Q - I \qquad [1]$$

where P is the cumulative rainfall [L^3]; Q is the cumulative outlet discharge [L^3]; I is the cumulative infiltration [L^3]; and ΔS is the depression storage change [L^3]. It was assumed that evaporation during the rain events was negligible and there was no vegetal interception for the bare soil surfaces. Therefore, the surface depression storage and infiltration were the total abstraction in the system. Using Eq. [1], the total infiltration during the rain event can be calculated by subtracting Q and ΔS from P (i.e., $I = P - Q - \Delta S$).

2.3. Results and Analysis

2.3.1. Puddle Delineation

The scanned surface DEM data were analyzed by the PD program and puddles and their combination relationships were delineated. Fig. 2.2 shows the DEMs of both rough and smooth field plots used in these experiments. The RP was divided into three major sub-basins based on the delineation results (Fig. 2.2a).

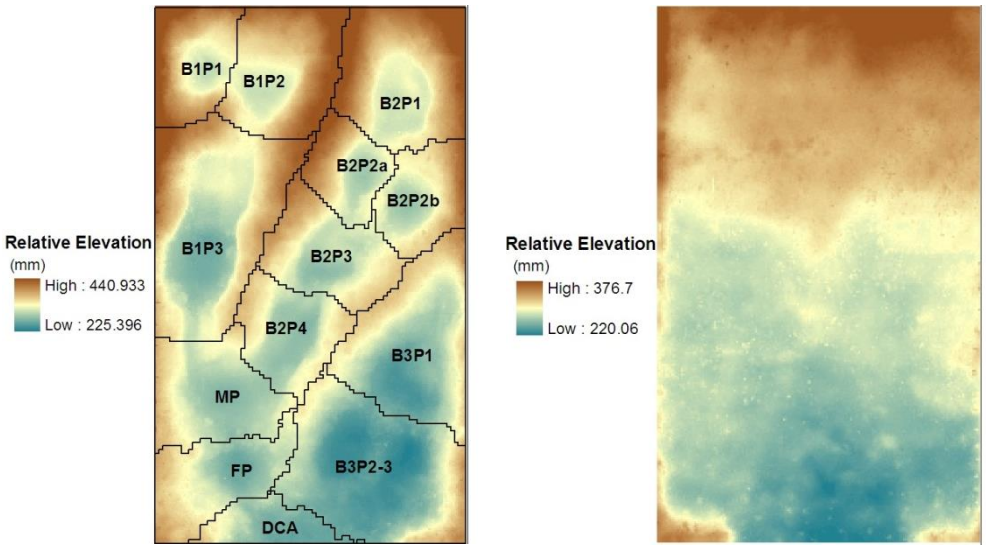

(a) Rough Plot Surface (b) Smooth Plot Surface

Figure 2.2. DEMs of the rough and smooth surfaces. The rough plot depicts contributing area boundaries for each puddle along with subbasin and puddle naming classification. Puddles are named by basin and upstream to downstream order (starting upstream) (e.g., Basin 1 Puddle 1 is B1P1). Special cases are Mutual Puddle (MP) and Final Puddle (FP)

A naming convention for the puddles was developed based on sub-basin family and their upstream to downstream order. Since sub-basins 1 and 2 shared common depressions at their downstream end, special names were given to these puddles. The most upstream puddle of the common puddles between Basins 1 and 2 was called the mutual puddle (MP). The final puddle before the outlet was final puddle (FP) (Fig. 2.2a). Finally there was an area of the RP that did not contribute to any depressions before reaching the outlet and was termed as directly connected area (DCA) (Fig. 2.2a). The relationships and properties of these puddles insofar as their contributing areas, combination relationships, and connectivity will be further discussed in subsequent sections. Fig. 2.2a displays the contributing area for each individual puddle on the RP surface. Additionally, Table 2.1 shows the contributing areas as a percentage of the total area for individual puddles that singly connect to flow (e.g., B1P3, B2P1, and B2P2a) and puddles in major combination relationships (e.g., B1P1

and B2P2). Fig. 2.2b depicts the SP surface. It is a generally even sloping plane towards the outlet with little surface roughness or depression storage.

Table 2.1. Individual and Combined Puddle Contributing Areas

Puddle	Area Coverage (%)
DCA	2.82
B1P1, B1P2 (combined)	13.58
B1P3	14.45
B2P1	10.15
B2P2a	4.05
B2P2b	4.97
B2P3	6.78
FP, MP, and B2P4 (combined)	19.03
B3P1, B3P2-3 (combined)	24.17

2.3.2. Soil Moisture

Soil moisture data were extracted from the sensors after each rainfall event occurred. The amount of data extracted covered the majority of time that these field plots were in operation. Fig. 2.3 displays the soil moisture readings during each event. The exact locations and the relative depths of the sensors displayed in Fig. 2.3 can be found in Fig. 2.1.

The minutely readings of the volumetric water content from the soil moisture sensors show generally small, if any, changes in the moisture content of both field plots (Fig. 2.3). The shallower moisture sensors did experience a rise in moisture levels shortly after rainfall began. The higher and relatively unchanging soil moistures of both of these events are very likely due to the covering of both plots before and after each rain event. As previously mentioned, to protect the surfaces a large thick impermeable tarp was fixed over each surface. Covering the surfaces appears to have trapped subsurface moisture that would have otherwise evaporated. In fact, the change in initial volumetric moisture content for any given sensor is within 4% between the two rainfall events. However, the general uniformity of the soil moisture between surfaces allows for a direct comparison between the events.

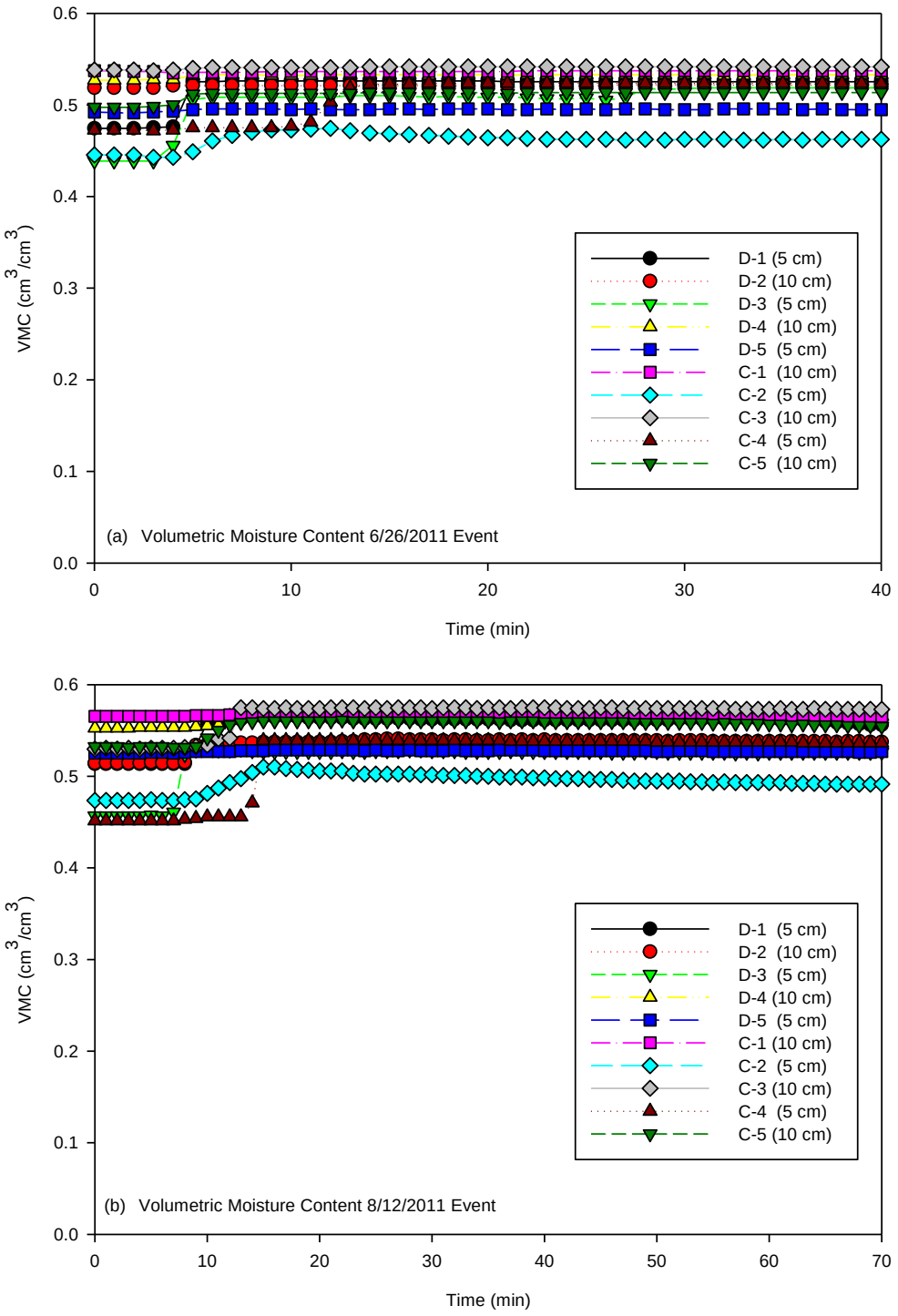

Figure 2.3. Volumetric water content readings from the soil moisture sensors during each rain event. Sensor depths below the soil surface are noted next to the sensor name. Time is relative to the beginning of rainfall for each rainfall event.

2.3.3. Hyetographs and Hydrographs

Two natural rain events on June 26 and August 12, 2011 had sufficient amount of effective rainfall to produce runoff for collection at the outlet of each field plot. Figs. 2.2 and 2.3 show the hyetographs and hydrographs of the RP and SP surfaces for the rain events 6-26-2011 and 8-12-2011, respectively. The average rainfall intensities were 1.28 cm/hr and 0.73 cm/hr for the hyetographs of Figs. 2.2 and 2.3, respectively. Both experiments indicated that the SP surface was more reactive to the rainfall intensity changes than the RP surface in generating flows at the outlet. That is, the smooth surface responded quicker to the rainfall input and produced more surface runoff, especially for the first high-intensity and short-duration rainfall event on June 26, 2011 (Fig. 2.4).

Both hyetographs (Figs. 2.4 and 2.5) show a generally similar rainfall pattern that had an initially shorter but higher intensity duration which was followed by a longer and lighter intensity rainfall. In the initial high intensity period, surface ponding condition occurred on both plots. However, this ponding and eventual surface runoff had different effects on the outlet hydrographs for the RP and SP surfaces. The smooth surface hydrographs for both events showed early spikes that corresponded to the initial heavy rainfall shortly after ponding occurred, after which the rainfall intensity dropped dramatically for both events and the SP flows reflected this change in both cases. With the exception of the incipient runoff delay caused by the infiltration dominant phase, the SP hydrographs largely mirrored the variations of their respective hyetographs of the two rainfall events. The RP hydrographs, however, experienced a long delay before they began to rise to any appreciable flow. As shown in the RP hydrographs, the flows rose considerably after the initial phase of high rainfall intensities, unlike the reaction of the SP.

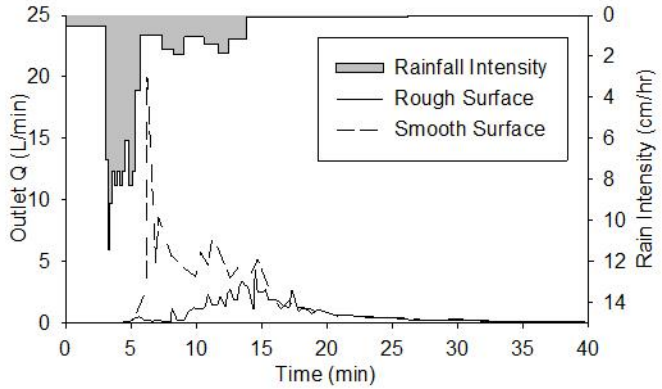

Figure 2.4. Hyetograph and hydrographs for the rough and smooth surfaces for rain event 6/26/2011 (note the differences in scale to Fig. 2.5)

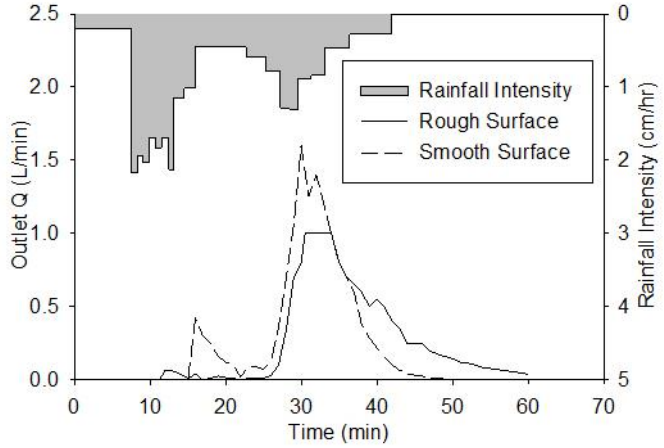

Figure 2.5. Hyetograph and hydrographs for the rough and smooth surfaces for rain event 8/12/2011 (Note the differences in scale to Fig. 2.4)

The cause of the difference in initial runoff was mainly due to the requirement to fully fill the storage of downstream puddles. This is in agreement with the findings of other studies that have suggested that the presence of surface depressions has a delaying effect on the initiation of runoff (Burwell and Larson 1969; Johnson et al. 1979; Helming et al. 1998; Darboux and Huang 2005). After the RP hydrographs of the two events began to rise, they somewhat deviated in their behavior. In the case of the higher intensity rainfall (Fig. 2.4), the flow steadily rose and reached a peak. The high point of this hydrograph corresponded with the end of the hyetograph (save for the extremely low intensity at the end of the rainfall

event). It was shortly after this point that the flows of both the RP and SP became equivalent in their slow descent. In contrast, the RP hydrograph of the low intensity event (Fig. 2.5) almost paralleled the curve of the SP hydrograph after its flow had risen appreciably. Both the RP and SP hydrographs seem to mirror the second rise and fall of their shared hyetograph. However, the RP flow was somewhat attenuated compared to the sharp crest of the smooth surface (Fig. 2.5). It is likely that the storage of the RP depressions has a reservoir routing effect on surface flow. The data showed that the SP hydrographs were generally more reactive to the changes in unsteady rainfall (Figs. 2.4 and 2.5). However, it is important to note the increased reactivity of the RP hydrograph to changes in the hyetograph of event 8-12-2011 (Fig. 2.5) over the much delayed flow of the RP hydrograph of event 6-26-2011 (Fig. 2.4) despite its lower overall rain intensity (Fig. 2.5).

2.3.4. Puddle Connectivity

The increases in flow caused by the increases in contributing area were analyzed by using the output from the PD program in conjunction with photographic evidence of surface events (i.e., puddle threshold breaches). Fig. 2.6 shows the increases in contributing area for the RP for both rain events. The sharp stepwise increases in contributing area are plotted against the cumulative rainfall. For both events, the observed puddle connectivity occurred in the same chronological order. This causes both contributing area curves to follow a similar general pattern. The cumulative contributing area percentages for these similar stepwise increases are 2.82%, 57.28%, 70.86% and 95.03% (Fig. 2.6). Table 2.2 shows the combinations of puddles, indicated in Fig. 2.2a, that represent these increases in contributing area. These depressions have been categorized by their connectivity. Due to the order and relationships of puddle connectivity observed, each partitioned group of depressions

simultaneously contributes to the outlet. This is caused by the downstream most depression reaching its threshold, allowing all connected upstream puddles to make contribution.

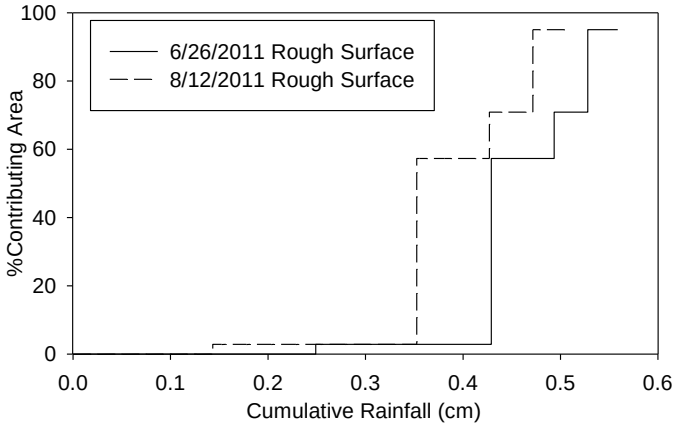

Figure 2.6. Contributing area increases of the rough surface versus cumulative rainfall for two events. 6-26-2011 (High intensity) and 8-12-2011 (Low intensity rainfall).

Table 2.2. Contributing Areas of Combined or Connected Depressions

Connected Depressions from Fig. 1a	DCA	B1P3, B2P1, B2P2a, B2P3, MP, FP,	B1P1, B1P2	B3P1, B3P2-3
Percentage of Total RP Surface Area	2.82	54.46	13.58	24.17
Percentage of Cumulative Connected RP Surface Area	2.82	57.28	70.86	95.03

The final row of Table 2.2 shows that the running sum of the contributing areas to the outlet collectively increases in a chronological order. Although the general pattern of connectivity is the same between the two events, it is interesting that the later event (8-12-2011) shows "quicker" connectivity than its earlier counterpart (Fig. 2.6). This implies that the depressions of the RP were filled with less rainfall volume input for the second event when compared to the first. The more easily induced connectivity has implications on runoff generation of the RP.

It should be noted that the total contributing area of the RP never reaches 100%. Puddle B2P2b (Fig. 2.2) never reached a fully filled condition for either event. However it did almost reach a fully filled status for both events so its depression storage is considered in

full for all intended purposes of this study. The first increase in contributing area percentage jumping from 0% to 2.82% (Fig. 2.6) accounts for a small area of the rough surface that drains directly to the outlet. The DCA area of the plot has no puddle threshold to overcome before contributing runoff. For this reason, the corresponding area increase associated with it is taken as the time that incipient runoff is collected at the outlet. However, all other increases can be understood by analyzing the photographic evidence (e.g., Fig. 1.1). There is an observable link between the surface connectivity and the accumulated flow at the outlet of RP for both events (Fig 2.4 and Fig. 2.7). Fig. 2.7 shows the accumulated outlet flow versus cumulative rain input for both surfaces of both events. Clearly, the first major increase in contributing area for the RP for both events (cumulative rainfall depths equal 0.43 cm and 0.35 cm for the 6-26-2011 and 8-12-2011 events, respectively) (Fig. 2.6) corresponds to the first significant rise in outlet flow (Fig. 2.7). Subsequent puddle connectivity beyond this point happens in a relatively short time frame for both events and is difficult to translate individually to the accumulated flow curve.

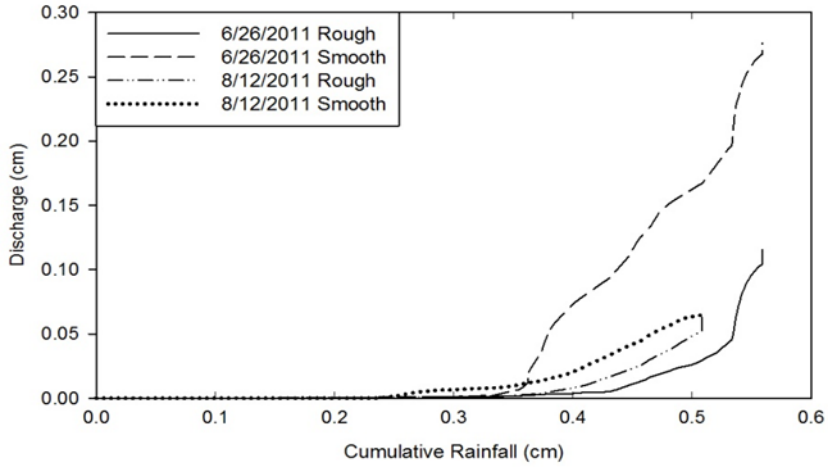

Figure 2.7. Cumulative outlet flow versus cumulative rainfall for the rough and smooth surfaces for rain events 6-26-2011 and 8-12-2011.

As previously mentioned, the connectivity of the RP was more easily induced in the second event. As a result, incipient runoff generation occurred with less rainfall input for the 8-12-2011 event. In fact, the runoff generated for the entirety of the 8-12-2011 event was higher for the same rain input than its earlier counterpart (Fig. 2.7). An opposite trend occurs when comparing runoff generation from the smooth surface between the two rainfall events. The SP surface produced markedly higher runoff for the earlier event after incipient runoff began to flow at the outlet. The 8-12-2011 event clearly has more comparable discharge volume curves than the 6-26-2011 event. These findings indicate that the runoff generation capability of the RP changed between the two events in a more drastic way than that of the SP. The following mass balance analysis further considers this notion.

2.3.5. Mass Balance Analysis

The compiled data of Table 2.3 allows for a basic mass balance analysis of runoff generation for both plots. Data presented in this table was generated from the DEMs of both surfaces, the rainfall collected by the tipping bucket rain gage, and the runoff collected at the outlets of the surfaces for each event. The differences between the contributions of the RP and SP for the first rainfall event (6-26-2001) (Table 2.3) were also observed in the runoff generation curves (Fig. 2.7). This is in contrast to the very similar total runoff volumes of both surfaces for the later rainfall event (8-12-2011).

If assuming that the infiltration characteristics of the two surfaces are similar, one would expect that the apparent infiltration of the RP would be equal to or slightly greater than that of the SP. However, in both cases the apparent infiltration of the RP is lower. Additionally, the differences in apparent abstraction between the two surfaces for both rain events are drastically different. The difference in abstraction for the later event is practically

negligible compared to the first event. This suggests two conclusions: (1) Specifically for these experiments, the overall infiltrability of the RP was lower than that of the SP for both events (Table 2.3). Thus, even though the RP seems to have lower overall infiltrability, the larger MDS kept it from generating more runoff than the SP. (2) The RP's infiltrability greatly decreased between the two events. This is further evidenced by the contributing area curves (Fig. 2.6) and the runoff generation curves (Fig. 2.7).

Table 2.3. Mass Balance Estimation for the Field Experiments

	Smooth surface		Rough surface	
	6/26/2011	8/12/2011	6/26/2011	8/12/2011
Cumulative rainfall (cm)	0.559	0.508	0.559	0.508
Total runoff (cm)	0.276	0.065	0.115	0.064
Estimated Abstraction (cm)	0.283	0.443	0.444	0.444
Maximum depression storage MDS (cm)	0.014	0.014	0.207	0.207
Estimated infiltration (Abstraction - MDS) (cm)	0.269	0.429	0.237	0.237
Runoff production as a percentage of total rainfall	49.40%	12.90%	20.60%	12.60%

A lower volume of rainfall was required to fill depressions and increase contributing area for the later rainfall event. Comparing the RP to the SP for the 8-12-2011 event, it seems possible that given a longer natural rain event the RP may have overtaken the SP in runoff production.

Previous studies indicate that under similar initial conditions (e.g., soil type and initial moisture content), higher rainfall intensities induce a more rapidly decaying infiltrability curve (Smith 1972; Diskin and Nazimov 1996). This would suggest that the higher intensity rainfall event should produce surface runoff earlier from a rain volume input standpoint. However, our data do not follow such a trend. It seems clear that the infiltration characteristics of the RP changed with a greater magnitude than the SP (Table 2.3), which caused a significant change in the amount of excess rainfall required to fill the

depressions of the RP (Fig. 2.6). This "quicker" connectivity gave rise to increased runoff generation during the 8-12-2011 event (Fig. 2.7).

We find our study to be in agreement with Gomez and Nearing (2005) and Darboux and Huang (2005) who posited that rough surfaces can experience a rising steady state flow with subsequent rain events. Gomez and Nearing (2005) concluded that higher hydraulic resistance to infiltration of a rough surface increased with subsequent rain events. This lower conductivity gave rise to the higher steady flows which shortly overtook the smooth surface in terminal runoff rates. Experimental studies have shown that microtopography has a definite effect on the spatial variability of hydraulic conductivity (Fox et al. 1998a; Fox et al. 1998b). Depressions, which act as a depression for detached soil particles (Cogo et al. 1983; Cogo et al. 1984), give rise to sediment induced surface sealing by acting as a depository for particles, causing sediment seals around puddle floors (Fox et al. 1998a; Fox et al. 1998b). Sediment seals have been shown to be considerably less hydraulically conductive than structural seals (Fox et al. 1998a) which are caused by the physical impact of rain on a surface. However, sealing effects are not the focus of this study. The findings of this study are related to those of Fox (1998a), and Nearing and Gomez (2005). However, the methodology and analysis executed in this study are vastly different from those in the aforementioned studies.

2.4. Summary and Conclusions

This research involved a field study on the effect of microtopography on runoff generation under natural rainfall conditions. Two plots were prepared in the field to highlight smooth and rough microtopographic conditions. One was populated with connected surface depressions and puddle connectivity from the upstream to downstream

and the other was an inclined plane surface. To quantify the topography, each surface was scanned using a high resolution laser scanner. The extracted DEM data were processed by using the PD software. The PD program calculated the maximum depression storage, the maximum ponding area based on a fully filled condition. The PD program was also used to quantify the contributing areas of major depressions over the rough surface. Two natural rain events (unsteady rainfall) were fully captured. Real time data, such as rainfall, outlet flow, and soil moisture contents were collected for each event. The topographic data were used in conjunction with the real time data collected for the two rainfall events in an attempt to characterize the threshold-driven overland flow processes. Comparisons of the changes in contributing areas and basic mass balance analyses were conducted for the two surfaces over the two rain events.

The experimental data showed that the smooth surface runoff output was, in general, more reactive to rain intensity variations than the rough surface for each respective event. However, the response of the rough surface runoff generation increased dramatically during the second event. Both events showed delay in appreciable flow growth for the RP due to the depression storage requirements. Late runoff from a rough surface relative to the smooth surface is a documented phenomenon (Burwell and Larson 1969; Johnson et al. 1979; Darboux and Huang, 2005).

Based on the mass balance analyses and the observed puddle connectivity, the effect of microtopography on runoff generation was found to be a dynamic process. Temporal changes in the apparent infiltrability of the rough plot surface narrowed the difference in runoff generation between the rough and smooth surfaces. Several studies have tried to determine whether rough or smooth surfaces will necessarily generate more runoff than the

other. Our experimental study indicated that runoff generation from the rough soil surface was subject to temporal changes and therefore no absolute answer can be plied to this question for any given scenario. However, it seemed that runoff generation between the rough and smooth surfaces likely began with the smooth surface dominating flow, and over multiple rain events the differential gap in runoff production narrowed or even possibly switched inequalities.

CHAPTER 3. LABORATORY OVERLAND FLOW EXPERIMENTS AND MODELING

3.1. Introduction

In this research, a wide range of experiments that considered microtopography in a controlled laboratory setting were executed. To better understand the effects of surface microtopography, experiments considering various hydrologic factors were executed using replicated rough and smooth surfaces. In this way, the effects of microtopography in conjunction with various conditions were analyzed. The factors considered in the laboratory experiments included soil type, rainfall intensity, and initial moisture content. These factors are important to any hydrologic analysis because of their influence on the partition of infiltration and surface runoff generation.

Simulations using the P2P modeling system (Chu et al. 2013) were performed for the conditions similar to the physical laboratory experiments. The results of the simulations and the observed experimental data were then compared. The P2P modeling system that incorporated a modified Green-Ampt model provided temporal and spatial hydrologic processes such as infiltration, surface ponding, and overland flow transfer.

3.2. Methods and Materials

3.2.1. Laboratory Materials and Equipment

Laboratory experiments that examined the effects of microtopography were executed in the Overland Flow Laboratory (OFL) under an array of varying conditions. The variables considered were soil type, initial moisture content, and rainfall patterns. To control these variables and quantify their effects on runoff generation, a process of experiment preparation which employed several pieces of important equipment had to be executed.

Raw soil was processed, wetted to a target moisture content, and packed into a soil box with a removable surface mold. The soil surface was scanned with the high-resolution laser scanner to extract its DEM. The soil box was placed under the rainfall simulator and experimentation was then executed.

3.2.1.1. Soils and Soil Processing

Three different soils were employed for the experiments in this research. These soils were silty clay, silty clay loam, and loamy sand. The textural breakdown of the silty clay was 11.9%, 42.0%, and 46.1% sand, silt, and clay, respectively. The silty clay loam consisted of 11.1%, 60.1%, and 28.8% sand, silt, and clay, respectively. Finally, the loamy sand was 80.3%, 14.6%, and 5.1% sand, silt, and clay, respectively. The silty clay loam and silty clay were both extracted from a farm near Buxton, ND. The loamy sand was extracted from a farm near Ulen, MN. According to the NRCS web soil survey, the soil in the area near Buxton, ND where the silty clay loam and the silty clay were extracted was shown to be a Bearden (Fine-silty, mixed, superactive, frigid Aeric Calciaquoll) silty clay loam. The soil in the area near Ulen, MN, from which the loamy sand was extracted, is shown as a Lohnes (Sandy, mixed, frigid Entic Hapludoll) loamy sand.

Depending on the aggregate strength of the raw soils, different methods of processing were employed to break down the soil aggregates to a more uniform and workable gradation. After extraction, the soil was left outside on large tarps until reaching an air dry state. Large soil aggregates were broken up by shovels and metal rakes. The loamy sand and the silty clay loam were then sifted through a 2 mm screen. The processed soils were then stored and subsequently used for the experiments. The silty clay was also sieved through a 2mm screen in a manner similar to the other soils. However, due to the

higher aggregate stability of the silty clay soil, this method of processing was less efficient. To process the leftover soil from the screening process, a soil grinder with a 2-mm sieve was employed.

Before any experimentation involving these soils was to be executed, the soil had to be brought to a desirable moisture content based on the design and objective of the experiment in question. A sample of the soil was weighed before and after a 12-hour duration in a 110 °C as per ASTM D-2216-10 (ASTM 2003). Once the air dry soil moisture was determined, a calculated volume of water was added to the soil based on the desired initial experimental water content and the desired bulk density of the packed soil. The calculated volume of water was mixed in with the soil and the soil pile was covered with tarps overnight to allow even moisture redistribution. The following day the soil was uncovered and packed into the soil box. Final moisture samples were also taken before packing soil to ascertain the actual moisture contents of the soil.

3.2.1.2. Soil Box and Soil Packing

Each laboratory experiment involved packing soil into a large soil box to be used under the rainfall simulator. The soil box was made from an angle steel frame that supported plexiglass walls and a wooden floor (bottom) to the box. It was set on heavy duty casters, making it mobile but also able to support the soil to be packed into the box. The soil box surface was 120 cm x 100 cm. However, the soil box was partitioned into two separate chambers using a removable plexiglass dividing wall that dissected the soil box equally. This allows a side-by-side comparison of different conditions for the same rainfall event. Specifically for this research, the divider was used to create two different microtopographic surfaces with similar subsurface conditions (e.g., initial moisture and soil

type). Both sections of the soil box had an equal top surface area of 100 cm × 60 cm. This particular soil box used detachable surface molds to create an identical soil surface for every experiment. This methodology of replicating soil surfaces was detailed by Sande et al. (2011). The soil box surface used a mold bracing system to fix the surface molds to the box. Fixing the surface molds to the box frame created a hollow space between the surface molds and the walls and floor of the soil box. It was in this void space that the soil would be packed into the soil box, allowing the relief of the soil to take the negative shape of the mold. The rough surface mold was created by constructing a small fame that was filled with cement. The cement was cured to be populated with mounds and depressions to create a rough surface characteristic across the soil surface. The smooth surface mold was made from a piece of flat plywood to create a smooth surface.

Once the rough and smooth molds were fixed to the angle steel frame of the soil box, it was then tilted onto its side at a 90° angle. Soil was then packed "laterally" into both the divisions of the soil box through the open "front" of the soil box. To ensure an even bulk density throughout the packed soil, soil was added in calculated amounts and packed to incremental "lifts." In this case, every soil "lift" was 5 cm up to the 1.0 m axis of the soil box. The amount of soil added for each lift on either partition was calculated based on the volume of the particular section of the soil box to be filled. The smooth surface had an equivalent mass of soil packed for each incremental lift while packing the soil box due to its shape and volume uniformity. This soil packing method ensured a uniform bulk density across the entire soil box (Sande et al. 2011). Variations in the volume of "lifts" over the rough surface necessitated a calculation of the amount of moisturized soil to be packed into

the box. This issue was relieved by a scan of the mold surface and computation of the volume displacements associated with surface microtopography by using the PD software.

Once both sides (rough and smooth surfaces) of the soil box were filled, the sidewall that was removed for soil packing was reinstalled which included the outlets of both the rough and smooth surfaces and runoff collection funnels. At that point, all walls of the soil box, including the surface molds, were fixed to the frame, and the soil box was still resting on its side. The soil box was then tilted back to the upright position using a large chain hoist to securely lower the soil box (Sande et al. 2011). The surface molds were unfastened from the frame of the soil box and removed. The soil box was then placed under the rainfall simulator.

Before applying rainfall to the surface of the soil box, the front end was fixed by applying brakes to the casters and lifting the back end of the soil box using hydraulic jacks. This allowed the slope of the soil surface to be manipulated to a desirable grade. For the experiments in this study, the slope of the soil box was always adjusted to 7%. After all final adjustments were made, the experiment began. During an experiment, observers collected runoff from the outlets of both the smooth and rough surfaces and also marked the locations of the wetting front along the sides of the soil box. Experiments were carried out until runoff from the outlet appeared to reach a steady rate. Steady flow from the outlet during steady rain application signified that the final infiltration capacity of the soil had been reached. After the end of each experiment, the soil that was used was removed from the soil box and disposed. Fresh processed soil was used for each experiment and no soil was reused for experimentation.

3.2.1.3. Rainfall Simulator

Experiments in the OFL were executed using the Norton-style rainfall simulator. This simulator was originally designed and built for erosional studies (Meyer and Harmon 1979; Meyer 1994). The designer's aim was to create a cost effective rainfall simulator that can accurately and repeatedly create a simulated rain that is similar to a natural storm. The considered design characteristics of the rainfall simulator were rain drop size distribution, rain drop velocity and distribution uniformity. The simulator uses an oscillating boom with four VEEJET 80100 nozzles (Meyer and Harmon 1979; Meyer 1994). The boom, which is operated by a gear box with a stop clutch mechanism, rotates in alternating directions causing a back and forth "sweep" of water spraying from the nozzles over the desired area. The gears which operate the boom are controlled by a switch box with an integrated software package that sets the sweep frequency and thus the "rain" intensity. The system is fed water by a large tank (1,900 liters). The pressure at the nozzles is critical to ensure not only that the flow distribution is uniform but also that the drop size distribution is similar to that of natural rainfall. The simulator covers over an area of 1.50 m × 4.50 m. The rainfall intensities are programmable, ranging from 0.97 to 10.42 cm/hr. This simulator produces a range of droplet sizes from 1 mm to 7 mm to imitate natural rainfall (Blanquies et. al 2003).

3.2.2. Laboratory Experiments

To study the effects of various aforementioned hydrologic experimental factors (i.e., initial moisture content, rainfall intensity and patterns, and soil type) in conjunction with microtopography, a set of experiments were designed and executed to consider individual hydrologic factors (e.g., soil type). Table 3.1 below archives the experiments that are compared to each other for each specified hydrologic factor.

Table 3.1. Physical Laboratory Experiments

Experimental Factor	Experiment	Soil Type	Rainfall Intensity (cm/hr)	Initial Moisture Content (cm^3/cm^3)
Soil Type	A	Silty Clay Loam	5.95	0.139
	B	Loamy Sand	5.95	0.144
	C	Silty Clay	5.95	0.120
Rainfall	D	Silty Clay	3.54	0.145
	E	Silty Clay	5.95	0.174
	F*	Silty Clay	5.95, 1.16, 3.54, 5.95	0.213
	G**	Silty Clay	5.95, 5.95, 5.95	0.226
Soil Moisture	H	Silty Clay	5.95	0.207
	I	Silty Clay	5.95	0.165
	J	Silty Clay	5.95	0.120

*Experiment performed using unsteady rainfall pattern. Intensities are listed in the chronological order applied during the experiment.
**Experiment performed under a complex rainfall pattern (i.e., multiple stages of rainfall alternating between wet and dry time periods). Note: three phases of rainfall using the same intensity.

Every experiment cataloged above used the aforementioned preparation methods. The first consideration of hydrologic parameters was the soil type involved. This factor is arguably one of the most important hydrologic considerations because soil type alone largely determines infiltration characteristics. Indeed, Rawls and Brakensiek (1983) provided a systematic way of estimating Green-Ampt soil infiltration characteristics based on available soil data. Higher quality estimations required fitting soil water retention curve points to the Brooks and Corey (1967) equation relating residual water content and air entry pressure. The air entry pressure can then be used to estimate the suction head (Bouwer 1969). At minimum, to estimate the characteristics required the textural class of the soil. Experiments A, B, and C (Table 3.1) for loamy sand, silty clay loam, and silty clay were compared under similar rainfall and initial moisture conditions to examine the effects of soil type.

The second area of focus was the effect of rainfall pattern and intensity in conjunction with microtopography. One soil type (silty clay) was used in a relatively small range of soil moistures under an array of rainfall conditions. These conditions included moderate steady, heavy steady, unsteady, and complex rainfall patterns (Experiments D through G, Table 3.1). The moderate and steady rainfall experiments (Experiments D and E) used single rainfall intensities for the duration of their respective experiments. In Experiment F, an unsteady rainfall was applied to both the rough and smooth surfaces of the soil box. The intensities applied, in succession, are listed in Table 3.1. The first rainfall intensity was applied until all areas of the rough and smooth surfaces were contributing runoff to their outlets. Under such a condition, all depressions of the rough surface were fully filled and their threshold points were breached with runoff. The smooth surface was under a ponding condition, giving rise to sheet flow over the surface. The final experiment (Experiment G) used in comparing rainfall applications in conjunction with microtopography considered a complex rainfall pattern. A complex rainfall pattern consisted of periods of rainfall and dry time in succession. In this case, three separate rainfalls were applied to the surface with extended periods of dry time between rainfall applications. These experiments provided some insight into the effects of rainfall intensity and pattern in conjunction with microtopography since both rough and smooth surfaces were employed in all cases.

The final hydrologic factor of interest in this set of experiments was the initial moisture content of the soil. A range of initial moisture contents were employed in a small series of experiments (Experiments H through J). One limitation on these experiments was the workability of the soil in the packing process and the color of the soil as a function of

moisture content. Soil that was too dry was generally unworkable and difficult to pack into the soil box. Workability was a factor in finding the initial moisture content to be used. Conversely, as a soil became moister it generally became darker in color. As soil became too dark, the wetting front became indistinguishable from unsaturated soil, rendering wetting front observations impossible. Therefore, a visible wetting front was the determining factor in the high end of the initial moisture contents.

3.2.3. Model Simulations Using the P2P Software

In addition to studying the comparative effects of microtopography on physical experiments, the results of some of these experiments were compared against the simulations of the P2P modeling system (Chu et al. 2013) regarding hydrologic processes such as infiltration, runoff production, ponding times, spilling times, and also storage consumption in the form of depressions over the surface.

3.2.3.1. Introduction to the P2P Modeling System

The P2P model simulates a series of dynamic puddle-to-puddle filling, spilling, merging, and splitting processes (Chu et al. 2013). Overall, the model accounts for the physical properties of depressions and quantifies the related threshold behaviors and hydrologic connectivity while simulating real time infiltration during rainfall events based on the DEM, soil, meteorologic, and other input data. To model the infiltration process, the P2P system incorporates a modified Green-Ampt model (Chu and Mariño 2005) that is applied to each cell within the DEM. The modified Green-Ampt model is capable of handling an array of various conditions, including homogeneous or heterogeneous soil profiles, steady or unsteady rainfall, and complex rainfall events. Additionally, the model

can handle shifting between pre-ponding and post-ponding conditions on a soil surface. It also provides temporal surface runoff production for any given cell.

While considering the modified Green-Ampt model for the vertical profile of every cell across a DEM, a surface may also be divided into different zones horizontally. Such divisions over the surface make the P2P system capable of regions of cells with different soil characteristics as well as non-uniform rainfall distributions. Given the capabilities of the modified Green-Ampt model along with the horizontal partitioning of the surface, the P2P system is capable of providing a comprehensive look at the detailed hydrologic process processes (e.g., infiltration and runoff production). Overland flow is routed through unique cell-to-cell (C2C) and P2P procedures for the DEM-based drainage system. The P2P modeling system provides a comprehensive outlook on many major aspects of the hydrologic process with respect to microtopography. The outputs of the model involve surface delineation, hydrologic connectivity, subsurface hydrology, mass balance, and surface hydrology. Within each of these major areas of hydrology, more specific outputs can be found. For example, surface delineation of the inputted DEM data yields information about the surface such as the MDS, MPA, puddle center cells, puddle thresholds, flow directions, flow accumulations, puddle geometric properties, etc. Additionally, 3D tools are also accessible to visually illustrate surface depressions and elevation variations. 3D animations can be created to show puddle connectivity relationships during the simulated process of puddle filling-spilling-merging, based on the model output. The hydrograph of the surface is also simulated and accessible through the model outputs. Within subsurface hydrology, the soil moisture profile along with the soil water velocity profile can be graphed for any cell in the surface. Finally, surface and subsurface mass balance simulation data can

be provided by the P2P model. The surface mass balance data ranges in scale from single cell calculations up to the entire surface.

3.2.3.2. Determination of Soil Hydraulic Parameters

The soil parameters required for the P2P modeling include the effective hydraulic conductivity, capillary suction head, saturated, residual, and initial water contents, soil retention parameters n and α, field capacity, and wilting point. The aforementioned soil parameters can be found by either physical experimentation or theoretical estimation. The effective hydraulic conductivity was initially estimated as half of the saturated hydraulic conductivity, as suggested by Bouwer (1969). To find the hydraulic conductivity, laboratory procedures were performed using a constant head permeameter method. The field capacity and wilting point parameters were found by measuring the matric potential of the soil at pressures of 33 kPa and 1500 kPa, respectively. The pressure plate and pressure cooker methods were used for finding the field capacity and wilting point of the soils, respectively.

Unlike the physically measured parameters, other soil parameters were found by theoretical estimation. The residual and saturated water contents, and the soil retention parameters n and α were estimated by using the Rosetta software package (Schaap et al. 2001). The Rosetta software uses a hierarchical approach to estimate such soil parameters (e.g., residual and saturated water contents, and soil water retention parameters) based on available user input data. The accuracy of the Rosetta's output is in part based on the level of user input data. The minimum amount of input data required by the user is the soil textural class for the desired output parameters. When provided with this level of data input, Rosetta's output is based simply on a lookup table. However, when provided with

higher levels of data (e.g. soil textural percentages, bulk density, field capacity, and wilting point), Rosetta uses various pedo-transfer functions to theoretically estimate the soil hydraulic properties from the aforementioned soil data. For this study, the highest level of input data for the Rosetta software was gathered and used. These inputs included the soil textural percentages, bulk density, field capacity, and wilting point. Based on this highest level of input data, Rosetta used the soil water retention estimation methods of van Genuchten (1980). Once all aforementioned hydraulic properties for each soil (silty clay, silty clay loam, or loamy sand) had been measured or theoretically estimated, they were inputted into the P2P model. All soil hydraulic parameters remained fixed in the model with the exceptions of the effective hydraulic conductivity and the capillary suction head. These two parameters were changed to make the best overall fits between the experimental and simulated results.

3.2.3.3. Comparison of Experiments and Model Simulations

Two metrics were used to evaluate the goodness of fit between the physical experiments and the P2P modeling simulations. These measures were the normalized objective function (NOF) (Ibbitt and O'Donnell 1971) and the model efficiency (EF) (Nash and Sutcliffe 1970). They can be respectively expressed as:

$$NOF = \frac{1}{\overline{X_O}} \sqrt{\frac{1}{n} \sum_{i=1}^{n} (X_{O,i} - X_{S,i})^2} \qquad [2]$$

$$EF = 1 - \frac{\sum_{i=1}^{n} (X_{O,i} - X_{S,i})^2}{\sum_{i=1}^{n} (X_{O,i} - \overline{X_O})^2} \qquad [3]$$

where X = state variable; $\overline{X}$= mean of X; n = total number of data points; and subscripts O and S denote the observed and simulated data, respectively.

The experiments shown in Table 3.2 were selected to be used as comparison events to the P2P model simulations. The main parameters for calibration were the effective hydraulic conductivity, suction head, and saturated water content. The final two experiments (8 and 9) listed in Table 3.2 used several soil boxes that were linked together.

Table 3.2. Physical Experiments Selected to Compare with Simulated Results from P2P Model

	Experiment	Soil type	Duration (min.)	Rainfall (cm/hr)	Initial water content (cm^3/cm^3)
Rainfall	1*	Silty Clay	44-14-13	5.95, 5.95, 5.95	0.226
Soil Type	2	Silty Clay Loam	40	5.95	0.174
	3	Loamy Sand	78	5.84	0.144
Soil Moisture	4	Silty Clay	40	5.95	0.207
	5	Silty Clay	44	5.95	0.165
	6	Silty Clay	61	5.95	0.12
Size**	7	Silty Clay Loam	36	5.51	0.16

*Experiment performed under a complex rainfall pattern (i.e., multiple stages of rainfall alternating between rainfall and dry time period). Note that three phases of rainfall had the same intensity.
**These experiments used several soil boxes fixed together to form an overall larger surface.

Generally, the laboratory experiments in the OFL employed one 1.0 m × 1.2 m soil box. Experiment 8 used two of those boxes fixed to each other to create a new soil box that was 2.0 m × 1.2 m. Experiment 9 used three soil boxes that were fixed to each other to create a box that was 3.0 m × 1.2 m. However, due to the much larger sizes of these two boxes, they could not be processed using the aforementioned method of packing (Sande et al. 2011). To prepare Experiments 8 and 9, the soil had to be packed by hand, forming a custom surface that was not created by a mold. Fig. 3.1 displays the DEMs of the four

surfaces used for the laboratory experiments and the P2P modeling. The surfaces in Figs. 3.1c-d both did not compare with any smooth surfaces, but were purely comprised of mounds and depressions.

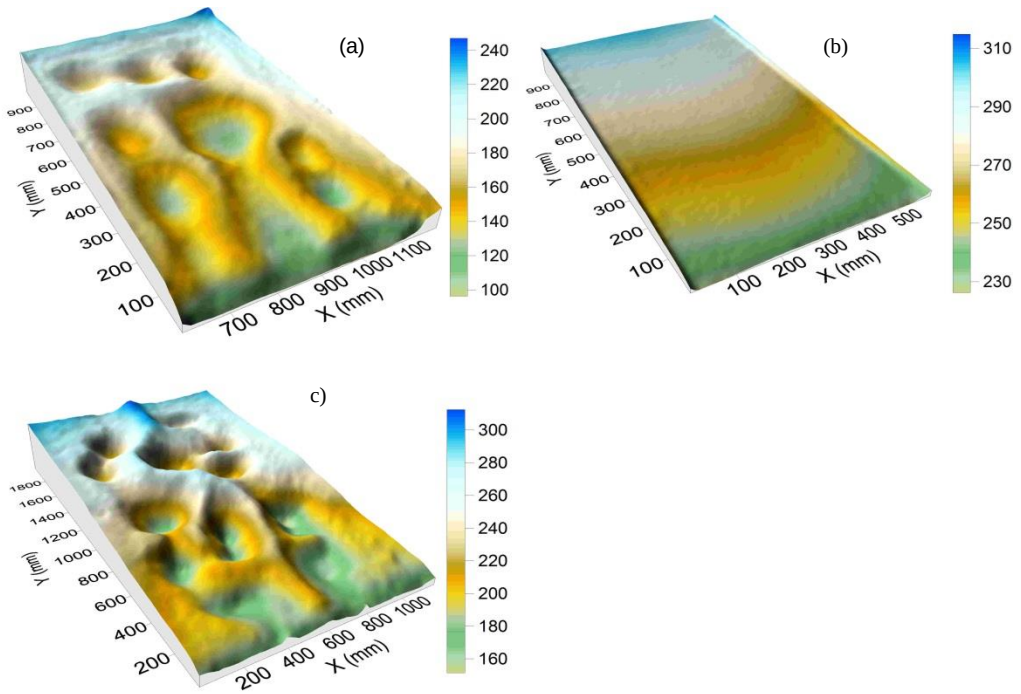

Figure 3.1. DEMs of topographic surfaces. (a) and (b) are renderings of the rough and smooth surfaces used in most laboratory experiments. (c) displays a rendering of the surface used for Experiment 7

3.3. Results and Analysis

3.3.1. Laboratory Overland Flow Experiments

3.3.1.1. Soil Type Effects

Experiments A, B, and C (Table 3.1) involved different soil types of varying textures and evaluation of their effects in conjunction with microtopography. The soil types used in these experiments were loamy sand, silty clay loam, and silty clay. While these soil types varied in textural breakdown, they were processed to have similar initial moisture contents (0.12 to 0.14 cm^3/cm^3) and were set under the rainfall simulator under the same rainfall

intensity (5.95 cm/hr) (Table 3.1). Fig. 3.2 shows the comparison of the observed hydrographs of the rough and smooth surfaces for the aforementioned Experiments A, B, and C.

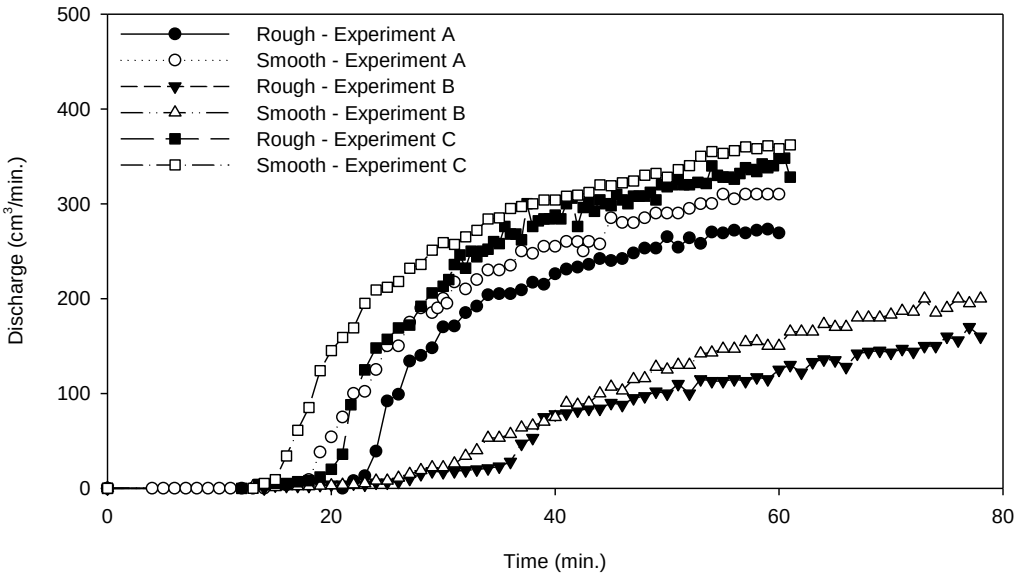

Figure 3.2. Comparison of the rough and smooth surface hydrographs for three soils (Experiments A, B, and C for silty clay loam, loamy sand, and silty clay soils, respectively)

The finer textured soils of Experiments A and C (silty clay loam and silty clay, respectively) behave more similarly than the coarser textured soil of Experiment B (loamy sand). The hydrographs of both rough and smooth surfaces for Experiments A and C are characterized by a sharp increase almost immediately after runoff begins at the outlet of the soil box. After the sharp increase in flow following the start of surface runoff, the flow begins to approach a near steady state for both surfaces. After roughly one hour of duration, the outlet discharge for Experiments A and C approaches to a steady state. The coarse textured soil of Experiment B shows both hydrographs taking a much steadier rise after initial runoff has occurred at the rough and smooth outlets of the soil box. However, the rough surface hydrograph does experience a significant increase in flow from a relatively

stable runoff rate at about 35 min. In this regard, the characterization of the hydrograph for the rough surface of the coarser textured soil is different from that of the silty and clayey soils. Additionally, both hydrographs are still rising as Experiment B ends after 80 min. under simulated rainfall conditions.

The rise in flow after initial runoff has been studied as a function of surface connectivity by some researchers (Moore and Larson 1979; Onstad 1984; Darboux et al. 2001; Darboux et al. 2002). Rough surface connectivity has been shown to dictate flow at the outlet. The early rise in the rough surface hydrographs of Experiments A and C is caused by the onset of their early and full surface connectivity. In this way, the rough surface hydrographs for these experiments are comparable to the smooth surface ones. Connectivity for these experiments was observed by marking the time that major depressions of the rough surface experienced threshold breaches and thus new area of the surface began to contribute surface runoff to the outlet. For Experiments A and C, most puddle threshold breaches of surface depressions occurred between 19 and 25 min. into the duration of the experiment. Puddle threshold spilling events for Experiment B were observed between 29 and 36 minutes with the last threshold event occurring at 67 min.

The low conductivity of the finer textured soils caused earlier ponding and thus earlier threshold flow time, causing "quicker" hydrologic connectivity. The earlier surface connectivity of the finer textured soils made the shape of the hydrographs appear more arc-like than the step-wise shaped hydrograph of the loamy sand (coarser textured soil) which had delayed connectivity. As a smooth surface ponds and begins to contribute runoff, the hydrograph of that surface should appear as steadily rising to reflect its growing connectivity until eventually leveling off due to full connectivity and a final infiltration rate.

A rough surface, however, will exhibit certain delays in runoff production depending upon the level of roughness and apparently the soil type. The results of these experiments indicated that the soil type affected the surface connectivity of the rough surface and by extension the characterization of the hydrographs.

Interestingly enough, in all cases (Experiments A, B, and C) the smooth surface generated a higher runoff rate and a higher volume of runoff than its respective rough surface. The idea that a rough surface will generate less total runoff than a smoother surface due to abstraction losses in surface storage is one that can be found in early papers (Johnson et al. 1979; Cogo et al. 1984). However, such a claim has been refuted by more recent work in this area (Helming et al. 1998; Darboux and Huang 2005; Gomez and Nearing 2005). It is important to note the differences in experimental setup among different studies. Many general factors are liable to vary between researchers' attempts in experimentation dealing in microtopography. Such factors include soil type, roughness levels, slope, rainfall intensity and patterns, scale, subsurface conditions, and roughness orientation. These factors alone have theoretical implications on runoff generation. In additional to these hydrologic parameters, the physical experimental apparatus may have some effect on the results of an experiment. For example, Helming et al. (1998) created their respective surfaces by hand, and used naturally occurring soil clods unlike our experiments which utilized a surface mold/packing method to create identical surfaces. Further, in some cases, the soil surface was pre-exposed to rainfall to initiate the surface sealing process (Darboux and Huang 2005).

3.3.1.2. Rainfall Effects – Steady Rainfall

Four different experiments aimed at the topic of rainfall intensity and pattern while comparing rough and smooth surfaces were conducted in this research. In all four cases (Experiments D, E, F, and G; Table 3.1), the soil type employed was a silty clay. The rough and smooth surfaces used for the experiments were also practically identical using the aforementioned packing methods of the soil box. In Experiments D and E, rainfall-runoff processes for the rough and smooth surfaces were compared under moderate and heavy rainfall events (3.54 cm/hr and 5.95 cm/hr, respectively) (Table 3.1) using similar initial moisture contents (0.17 - 0.18 cm^3/cm^3). Fig. 3.3 displays the comparison of the rough and smooth surface hydrographs for the moderate and heavy rainfall events.

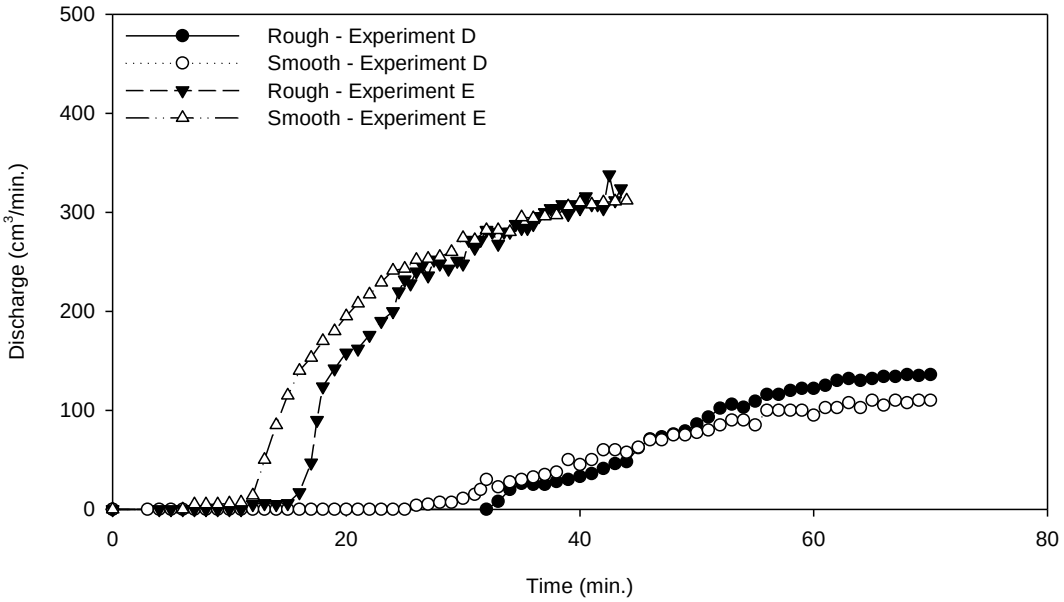

Figure 3.3. Comparison of the rough and smooth surface hydrographs under 3.54 cm/hr rainfall (Experiment D) and 5.95 cm/hr rainfall (Experiment E) using a silty clay soil.

The effect of rainfall intensity for both experiments generally shows that the lower intensity rainfall takes longer to reach a steady state at the outlet. Also in both cases, flow

from the rough surface is slightly delayed in rise compared with the smooth surface. Interestingly enough, the rough surface during the moderate rainfall experiment (Experiment D) overtook the smooth surface in runoff generation (Fig. 3.3). The final steady flows of the rough and smooth surfaces for the heavy rainfall experiment were essentially equivalent towards the end of Experiment E.

Similar to the comparison of the fine and coarse textured soils, there was a difference in the range of time for connectivity over the rough surface. The rough surface of Experiment E experienced delayed incipient runoff due to low connectivity. The flow at the outlet began to rise once increased total connectivity was realized over the surface in the range of 12 to 19 min. into the experiment (Fig. 3.3). The rough surface for experiment D utilizing the moderate rainfall intensity experienced most of its connectivity over the surface in the time range of 35 to 53 min. (Fig. 3.3). It seems intuitive that a higher intensity rainfall would fill depressions sooner and therefore have more rapid development of hydrologic connectivity, assuming similar infiltration characteristics. However, similarly to the previous analysis, this quick transition from little connectivity to full connectivity over a rough surface appears to give the hydrograph a smoother arc like curve that is comparable to that of a smooth surface. However, the rainfall with moderate intensity does not appear to give as quite as a dramatic "step-wise" shape to the rough surface hydrograph for Experiment D when compared with Experiment B for the loamy sand. The lower surface flow caused less of a noticeable surge at the outlet during connectivity events, giving rise to a steadier rising hydrograph.

3.3.1.3. Rainfall Effects - Unsteady Rainfall

Experiment F considered an unsteady rainfall event (Table 3.1). Such an event allows for the observation of both the ponding and non-ponding stages during rainfall given high and low intensities. Fig. 3.4 displays the hydrographs for both the rough and smooth surfaces under an unsteady rainfall pattern.

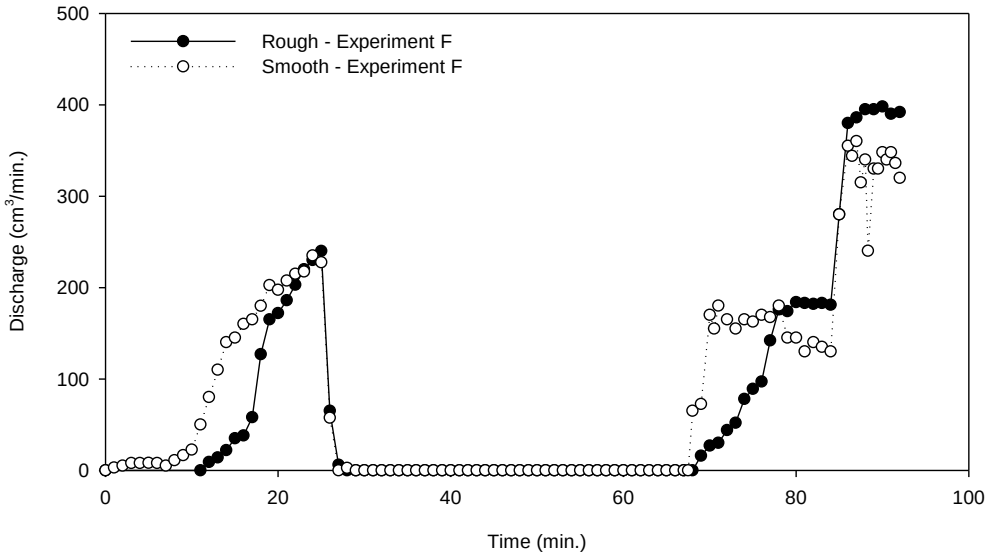

Figure 3.4. Comparison of the rough and smooth surface hydrographs for an unsteady rainfall pattern. Rainfall intensities in chronological order were 5.95 cm/hr, 1.16 cm/hr, 3.54 cm/hr, and 5.95 cm/hr for 25.0, 42.5, 16.5, and 8.0 minutes, respectively.

This experiment is unique to most physical experiments that are involved in microtopography research. The rainfall intensity began at 5.95 cm/hr over both smooth and rough surfaces and continued until all areas were contributing runoff to the outlet. The first portion of the hydrograph (Fig. 3.4) under the first intensity shows a typical comparison of hydrographs between rough and smooth surfaces. Again, the delayed connectivity of the rough surface, due to depression storage abstraction, delays the rise in its flow. However, at full connectivity over the surface, approximately 25 minutes, the flows from both the rough and smooth sides of the soil box are at comparable values. At that time the intensity of the

rainfall was set to the lowest setting possible which applied rainfall at a rate of 1.16 cm/hr. This low rainfall intensity was below the infiltration capacity of the silty clay soil that was used in this experiment, which was discovered through trial and error in small testing prior to the experiment. These conditions allowed both surfaces to enter a non-ponding condition which halted runoff collection at the outlet. Then, water that was being stored on the rough surface in depressions began to infiltrate. From the time that the rainfall intensity was reset to a lower application rate to the one when no ponded water could be seen on the surface, it took 42.5 minutes. Once the entirety of both surfaces had no ponded water, the intensity was then switched to 3.54 cm/hr. This rainfall intensity was higher than the infiltration capacity at this point in the infiltration process and therefore caused an instantaneous ponding condition. The hydrograph of the smooth surface reflects that the surface reached a fully contributing condition nearly instantaneously (Fig. 3.4). While also generating excess rainfall, the rough surface had to fill its depressions with water before it could reach a fully contributing stage. This is apparent in the hydrograph by the delayed rise (Fig. 3.4). Once both surfaces were again fully contributing to the outlet (after 16.5 minutes), the intensity was set to 5.95 cm/hr. This final intensity was used until an apparent steady flow at the outlet was evident (8 minutes) and then the experiment ended. The most revealing portion of these two hydrographs in Fig. 3.4 lies in the last two intensities of rainfall. During the period in which the rain intensity was 3.54 cm/hr, the flows both reach a steady state of near 180 cm^3/min with some variation observed on the smooth surface hydrograph (Fig. 3.4). However, once the rainfall was switched to a higher intensity, the rough surface had a markedly higher runoff rate than the smooth surface. It is important to note the clear difference in runoff generation between the two surfaces once a fully contributing status has

been reached. Similar to the field study experiments, over time the rougher surface generated as much or more runoff than the smooth surface. Experiment G will verify a comparative increase in the runoff generation on rough surfaces over the course of several rainfall events. These findings are in line with those from the field study.

3.3.1.4. Rainfall Effects - Complex Rainfall Series

The final set of experiments that cover rainfall intensity and pattern comparisons are the complex rainfall series. The complex rainfall series is one that experiences a dry time period between rainfall events. Figs. 3.5 – 3.7 show the comparison of the hydrographs for three separate rainfall events consecutively applied to its surface.

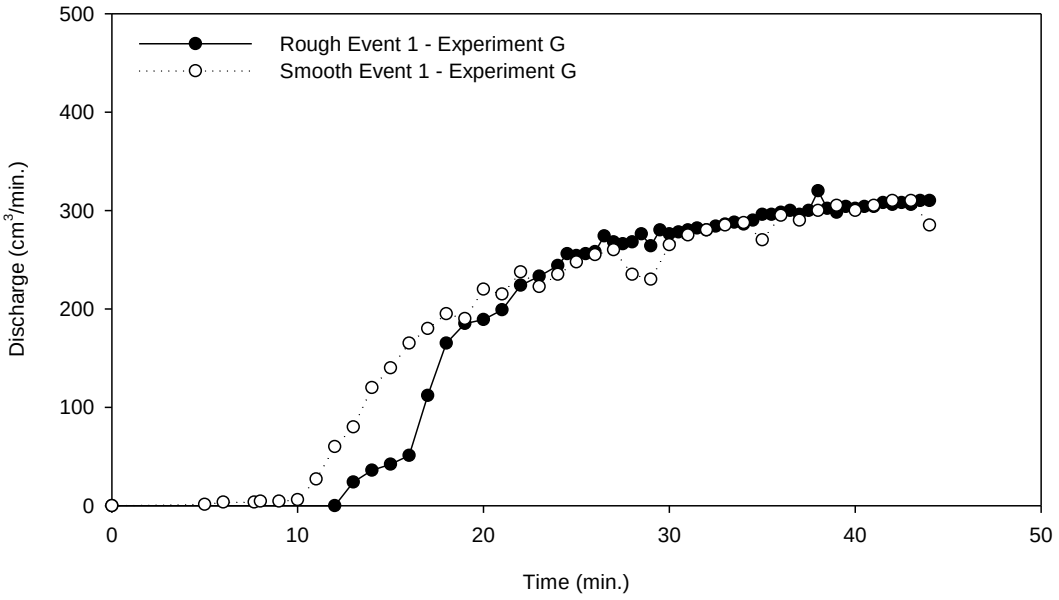

Figure 3.5. Complex rainfall event 1: rough and smooth surface hydrographs using a silty clay soil.

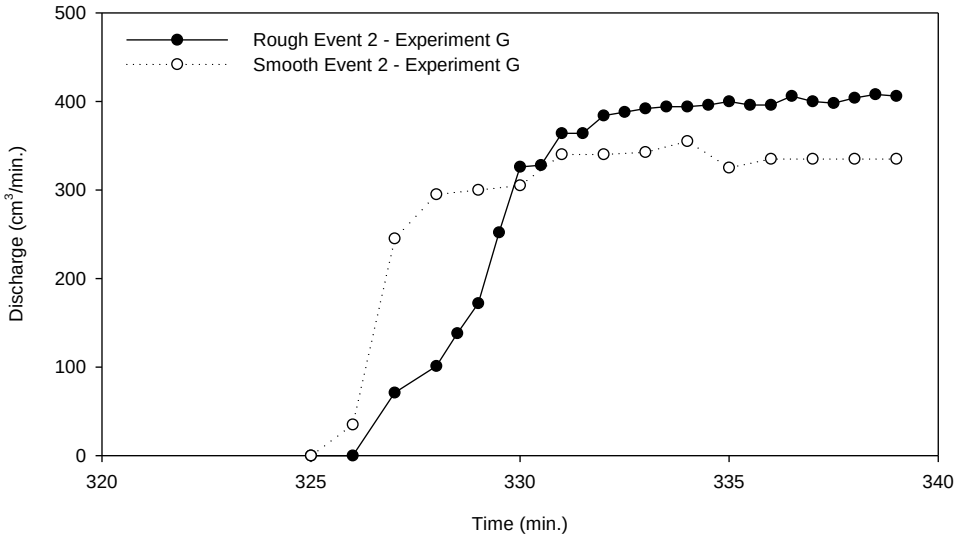

Figure 3.6. Complex rainfall event 2: rough and smooth surface hydrographs using a silty clay soil. (Note that time axis is relative to the beginning of the first rainfall event).

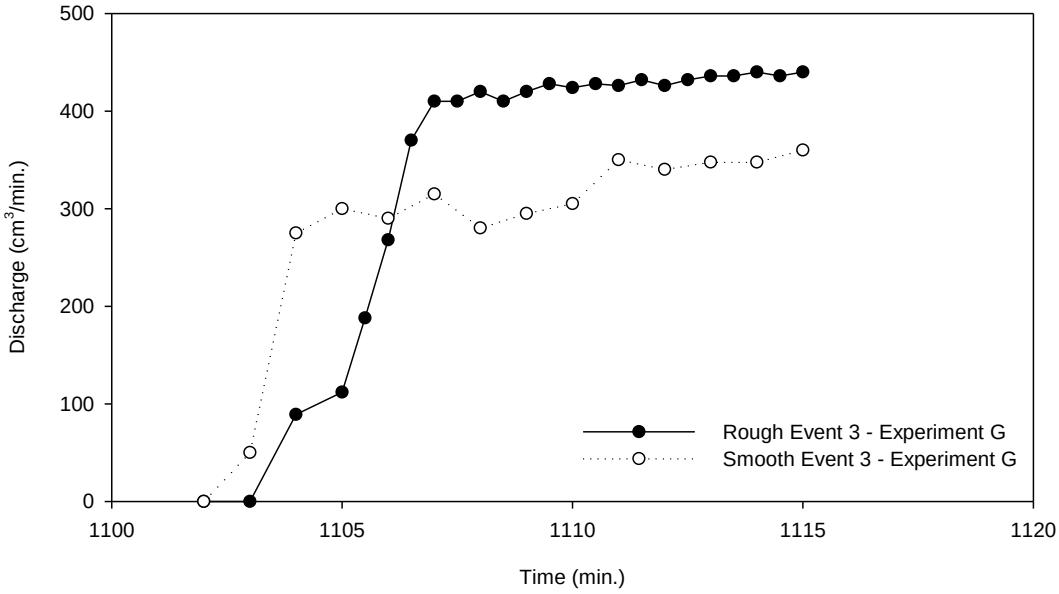

Figure 3.7. Complex rainfall event 3: rough and smooth surface hydrographs using a silty clay soil. (Note that time axis is relative to the beginning of the first rainfall event).

The first event of the complex rainfall series (Experiment G, Table 3.1) has rough and smooth hydrograph characteristics that are similar to the first rainfall intensity of the unsteady rainfall event (Experiment F) and the hydrographs of Experiments E. The rough surface hydrograph shows a delayed flow, compared with the smooth surface hydrograph. Also similar to the aforementioned experiments, the flows become comparable between both surfaces after complete hydrologic connectivity has been achieved. The data thus far suggest that runoff generation during an initial rainfall event, using fresh soil (i.e., soil that is packed into the soil box and experiences no rainfall), will either favor the smooth surface or will be similar between the surfaces. However, as previously shown during the later portion of rainfall for Experiment F (Fig. 3.4), a temporal effect of the runoff generation of the rough surface will take place and change the dynamic between outputs of the two surfaces. In fact, observing the differences in runoff differences between events 2 and 3 of Experiment G (Figs. 3.5 - 3.7) shows that the infiltration characteristics continue to change. The difference in steady state runoff rates, and by extension runoff production, between the rough and smooth surfaces is greatest for event 3, noticeable in event 2 and essentially nonexistent in event 1.

As previously mentioned, the field study portion of this research had similar findings through multiple natural rainfall events on field plots. The findings of the unsteady and complex rainfall events in this research show that the differences in runoff generation between rough and smooth surfaces are most certainly affected by temporal changes in the infiltration characteristics of the rough surface.

3.3.1.5. Initial Soil Moisture Effects

The silty clay soil was packed into the soil box for several experiments under different initial moisture conditions. Fig. 3.8 shows the compiled hydrographs of the rough and smooth surfaces for three different initial moisture contents.

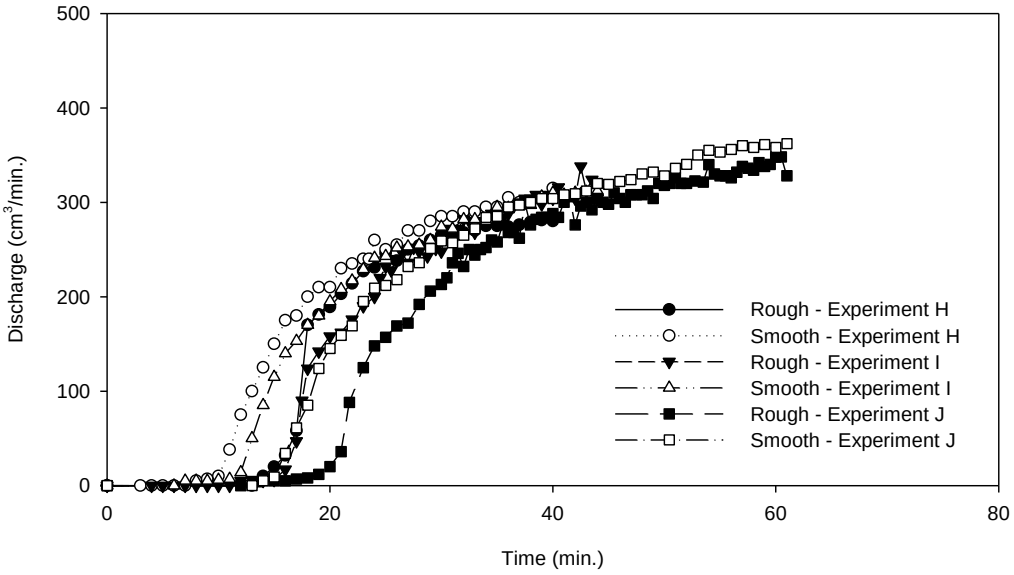

Figure 3.8. Rough and smooth surface hydrographs of Experiments H, I, and J using initial moisture contents of 0.207, 0.165, 0.12 cm^3/cm^3, respectively.

Increasing the moisture content does appear to cause generally faster runoff generation on both rough and smooth surfaces. Additionally, drier moisture contents take longer to reach an apparent steady state of outlet discharge. In all cases the rough surface maintains a flow rate lower than or equivalent to the smooth surface. This includes the final apparent steady state flows towards the end of each experiment. When considering the outcome of these experiments with the aforementioned ones, a casual trend can be observed. During an initial rainfall event, the smooth surface has a higher potential to generate runoff. However after an initial rainfall has passed, the runoff generation characteristics of the

rough surface begin to shift and it is potentially able to generate more runoff than the smooth surface despite its higher depressional storage.

3.3.2. P2P Modeling

3.3.2.1. Complex Rainfall Series Comparisons

Comparing the results of the P2P model against the physical laboratory experiment generally shows that the model is well suited to simulate overland flow and unsaturated flow over surfaces of different microtopographic characteristics for the first rainfall event. Fig. 3.9 displays the observed and simulated hydrographs for Experiment 1 (Table 3.2). While Figs. 3.9 a1 and b1 (Event 1) show well-fitting simulated hydrographs to the observed hydrographs, the simulated results show lower flow values for the rough surface (Figs. 3.9 a2-a3). However, there is not a clear difference in the final runoff rates of the smooth surface between the observed and simulated hydrographs for Experiment 2 (Figs. 3.9 b2-b3). From the analysis for Experiment G (Figs. 3.5-3.7), a comparison may be drawn to the differences in runoff generation between the rough and smooth surfaces. It seems that the ability of the rough surface to generate runoff changes between rainfall events yet the theoretical model can still accurately predict the hydrograph for the smooth surface.

Therefore, parallel can be drawn from one of the major conclusions of chapter 2 dealing in the changes of runoff generation differences between surface types and subsequent events. The goodness of fit of the simulated and observed outlet discharges is quantitatively evaluated by using NOF and EF and the results are displayed in Table 3.3. In both cases the EF values are very close to one which reflects a perfect match between the two data sets. Additionally, the NOF ranges from fairly low values for the first event

indicate good agreement between the simulations and the physical experiments.

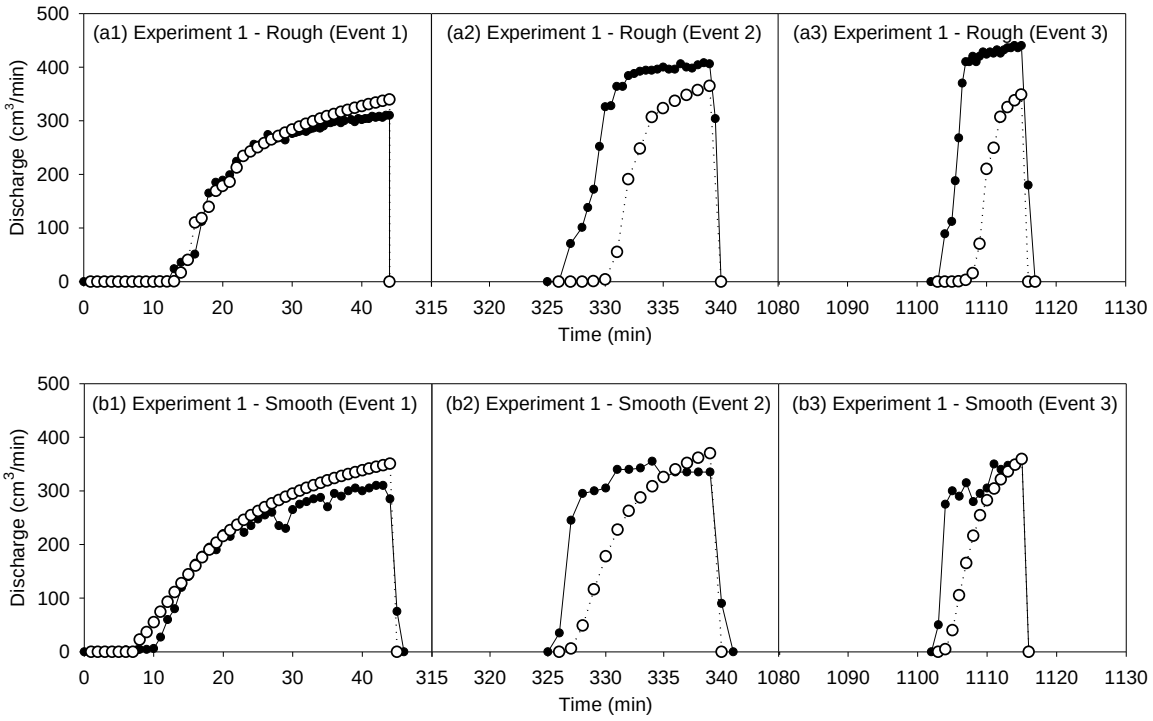

Figure 3.9. Comparison of the observed and simulated hydrographs for Experiment 1 during a complex rainfall series on silty clay

Table 3.3. Normalized Objective Function (NOF) and Modeling Efficiency (EF) Values of the Observed and Simulated Discharges for event 1 of Experiment 1

Surface		Rough	Smooth
Experiment 1, Event 1	NOF	0.10	0.16
	EF	0.98	0.94

Fig. 3.10 shows the comparison of the observed and simulated ponding and spilling times of the depressions of the rough surface for Experiment 1. Note that Fig. 3.10 shows the results of only the first rainfall event. The comparisons generally show that the ponding and spilling times are accurately modeled by the P2P process.

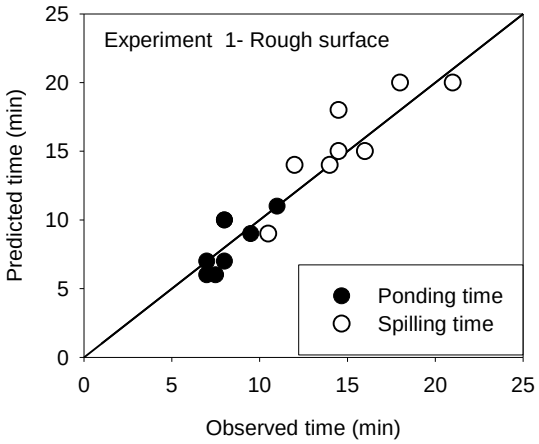

Figure 3.10. Comparison of the observed and simulated ponding and spilling times for rain event 1 of Experiment 1 using a silty clay soil.

3.3.2.2. Soil Type Comparisons

Based on the data from Experiments 2 and 3 (Table 3.2), P2P modeling was conducted to simulate the hydrologic processes for two different soil types: silty clay loam and loamy sand, respectively. The P2P model did accurately simulate the rough surface hydrographs of Experiments 2 and 3 (Figs. 3.11a1 and 3.11b1). The simulated rough surface hydrographs show stepwise changes which are also somewhat represented in their observed counterparts. These almost instantaneous changes in the flow rate are due to the filling and spilling process in depressions over the surface. As the water level of a puddle reaches its threshold, the puddle and its draining area begin to contribute flow to the outlet (assuming that it is then fully hydraulically connected). The concept of stepwise contributing area growth, and by extension runoff generation, was put forth by Moore and Larson (1979). A reasonable agreement is found between the simulated and observed hydrographs of the smooth surface for these experiments, particularly for Experiment 2 (Figs. 3.11a2 and 3.11b2).

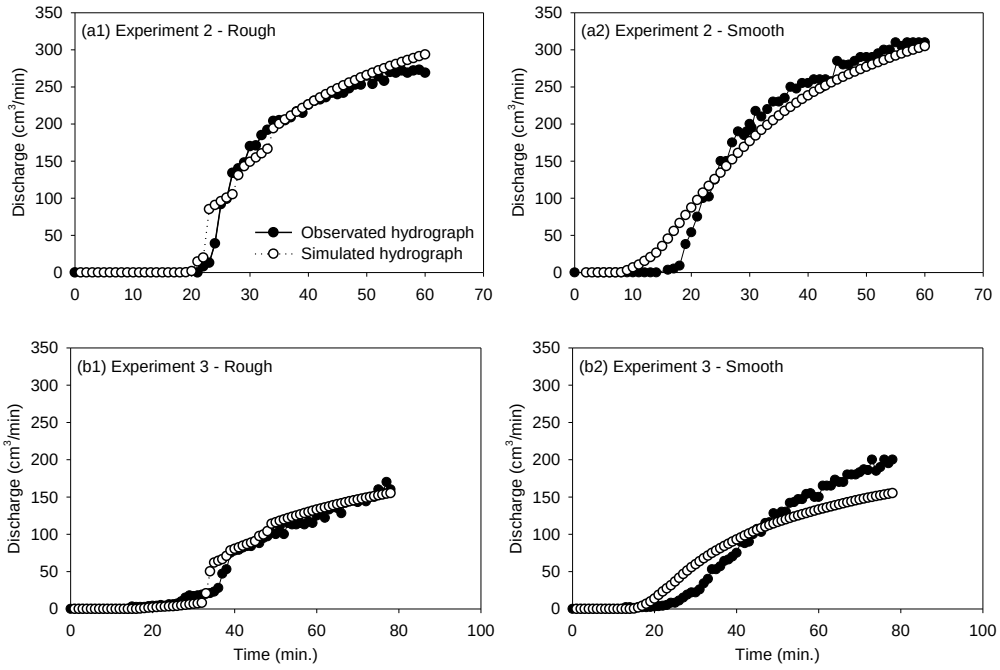

Figure 3.11. Comparison of the observed and simulated hydrographs for Experiments 2 and 3, using a silty clay loam and loamy sand, respectively.

Generally, the NOF and EF values show that the model reasonably predicted the runoff generation rates given the soil parameters and rainfall input (Table 3.4). However, certain discrepancy can be observed in the simulated and observed flows of the smooth surface for Experiment 3 (Fig. 3.11b2). As shown in Table 3.4, the associated EF and NOF are only 0.81 and 0.56, respectively.

Table 3.4. Normalized Objective Function (NOF) and Modeling Efficiency (EF) Values of the Observed and Simulated Discharges for Experiments 2 and 3

Surface		Rough	Smooth
Experiment 2	EF	0.99	0.98
	NOF	0.12	0.13
Experiment 3	EF	0.96	0.81
	NOF	0.26	0.56

Fig. 3.12a shows good agreement between the simulated and observed filling and spilling times of the rough surface for Experiment 2 utilizing the silty clay loam. However,

the loamy sand soil surface for Experiment 3 (Fig. 3.12b) does show some variations between the observed and simulated critical times. Generally the ponding time appears to be underestimated by the model for the loamy sand (Fig. 3.12b).

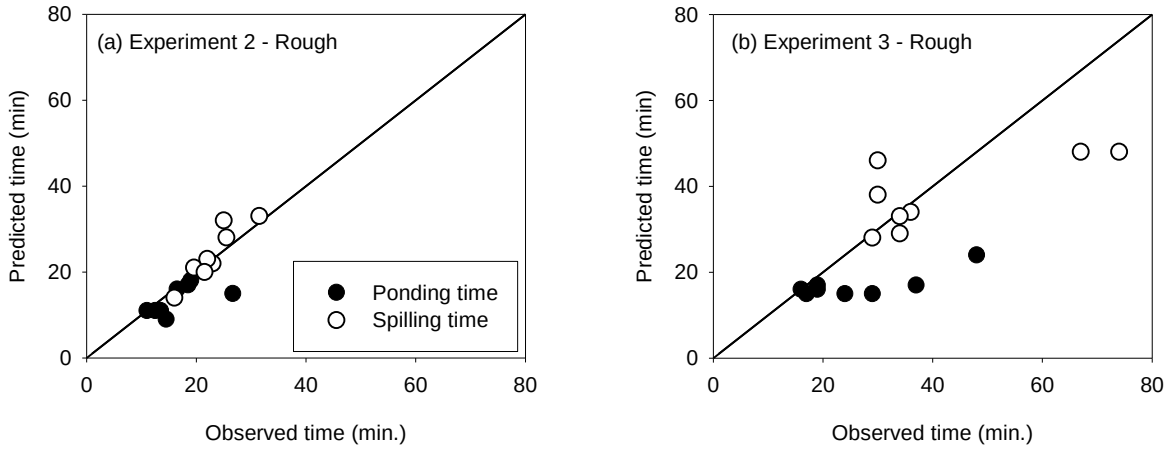

Figure 3.12. Comparison of the observed and simulated ponding times spilling times for Experiments 2 and 3 using a silty clay loam and loamy sand, respectively.

Fig. 3.13 displays a comparison of the simulated and observed average wetting front results for Experiments 2 and 3. Table 3.5 displays the comparisons results (EF and NOF) for the wetting fronts simulated by the model and the ones measured in Experiments 2 and 3 (Table 3.2). Extremely high EF values and very reasonable NOF values have been obtained, particularly for the loamy sand of Experiment 3 (Table 3.2). The results of these comparisons show that the P2P model is capable of simulating the P2P overland flow dynamics and unsaturated flow across varying soil types.

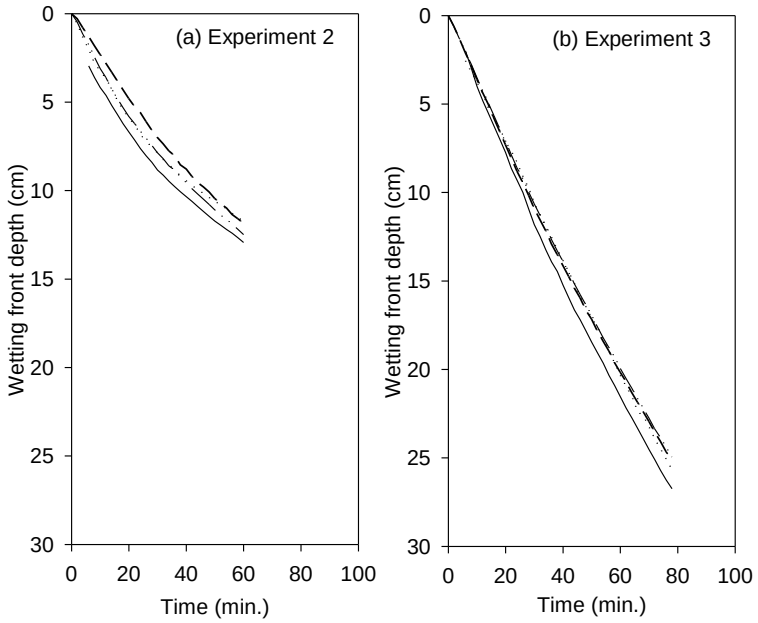

Figure 3.13. Comparison of the simulated and observed average wetting front depths for Experiments 2 and 3, using a silty clay loam and loamy sand, respectively.

Table 3.5. Normalized Objective Function (NOF) and Modeling Efficiency (EF) of the Observed and Simulated Average Wetting Front Depths for Experiments 2 and 3

Surface		Rough	Smooth
Experiment 2	EF	0.94	0.95
	NOF	0.12	0.12
Experiment 3	EF	0.98	0.99
	NOF	0.10	0.02

3.3.2.3. Initial Soil Moisture Conditions

The conditions for Experiments H, I, and J were all simulated by the P2P model and the modeling results were compared with the corresponding observed data. Fig. 3.14 shows a very good agreement between the simulated and observed results for these experiments. In all cases, the rough surface contributes a less or equivalent amount of runoff at the final steady state than the smooth surface for both observed and simulated flows. Such an outcome could practically make sense. At the steady state flow stage in these experiments,

the rough surface would need to be fully connected. Under the fully filled condition, inundated puddles could induce more infiltration. This conclusion is not necessarily at odds with what has been seen regarding the changing infiltration characteristics over the rough surface over the course of multiple rainfalls. These experiments took place on fresh soil which had not been subject to any previous rainfall and therefore bare soil infiltration characteristics between the rough and smooth surfaces can be assumed to be similar.

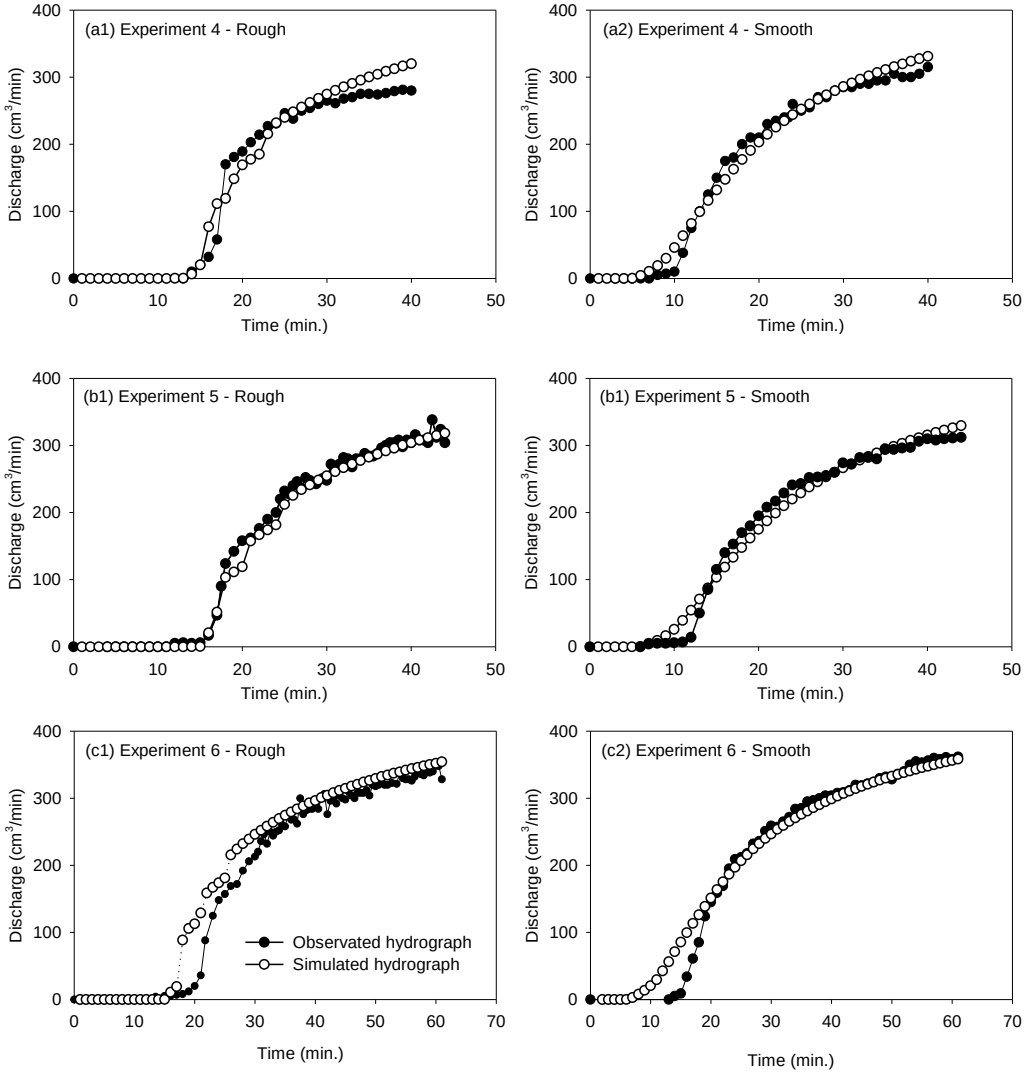

Figure 3.14. Comparison of the observed and simulated hydrographs for Experiments 4-6, using a silty clay soil and comparing initial moisture contents of 0.207, 0.165, 0.12 cm^3/cm^3, respectively.

NOF and EF values for Experiments 4 – 6 are displayed in Table 3.6. In general, these numbers confirm a very good agreement between the modeling results and the observed data. Particularly, the EF values reported show a strong agreement between the simulations and the experimental results. The NOF values for Experiments 5 and 7 are moderate.

Table 3.6. Normalized Objective Function (NOF) and Modeling Efficiency (EF) of the Observed and Simulated Discharges for Experiments 4-6

Surface		Rough	Smooth
Experiment 4	NOF	0.15	0.16
	EF	0.97	0.95
Experiment 5	NOF	0.07	0.08
	EF	0.99	0.98
Experiment 6	NOF	0.14	0.10
	EF	0.97	0.98

The critical ponding and spilling times of Experiments 4 – 6 are shown in Fig. 3.15. Similar to the hydrographs of these experiments, good agreement is found between the simulated and observed critical times. However, the model does underestimate all critical times for Experiment 6 (Fig. 3.15c). The comparison of the simulated and observed wetting front movement and metrics of model are displayed in Fig. 3.16 and Table 3.7, respectively. It is noticeable that the average observed wetting front data are missing during the beginning of the experiment for the rough surface. Due to a structural member that is required for the stability of the plexiglas walls of the soil box, a small portion of the soil column was covered. The member caused measuring the wetting front to become difficult during that portion of the experiment. In all cases, the model somewhat underestimated the average wetting front depths across both the rough and smooth surfaces. The differences between the simulated and modeled wetting fronts do however seem to narrow as each experiment progresses. The EF and NOF values of the experiments seem reasonable (Table 3.7).

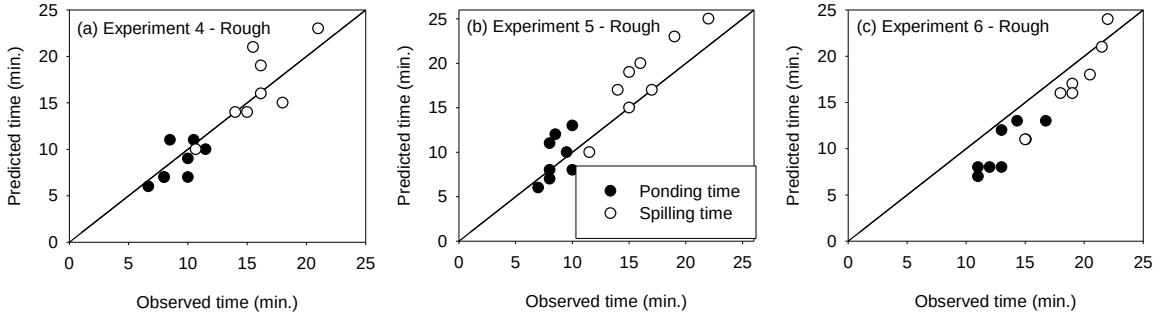

Figure 3.15. Comparison of the observed and simulated ponding times spilling times for Experiments 4, 5, and 6, using a silty clay soil and comparing initial moisture contents of 0.207, 0.165, 0.12 cm^3/cm^3, respectively.

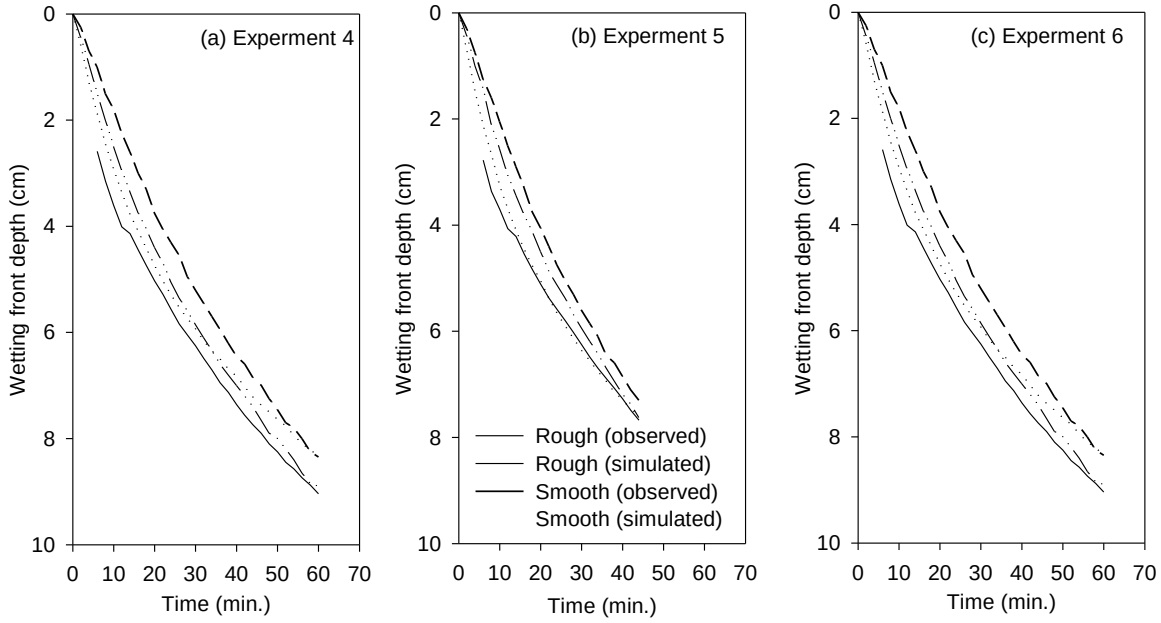

Figure 3.16. Comparison of the simulated and observed average wetting front depths for Experiments 4 – 6, using a silty clay soil and comparing initial moisture contents of 0.207, 0.165, 0.12 cm^3/cm^3, respectively.

Table 3.7. Normalized Objective Function (NOF) and Modeling Efficiency (EF) of the Observed and Simulated Average Wetting Front Depths for Experiments 4-6

Surface		Rough	Smooth
Experiment 4	EF	0.70	0.80
	NOF	0.17	0.20
Experiment 5	EF	0.78	0.72
	NOF	0.13	0.19
Experiment 6	NOF	0.90	0.89
	EF	0.11	0.15

3.3.3. Other Laboratory Surface

One other laboratory surface was used for a physical experiment (Experiment 7, Table 3.2) and P2P modeling. The simulated hydrograph for the experiment seems to have a relatively decent fit to the observed hydrograph (Fig. 3.17). Fig. 3.18 shows that the critical ponding and spilling times do vary somewhat between the modeled and observed results for Experiment 7.

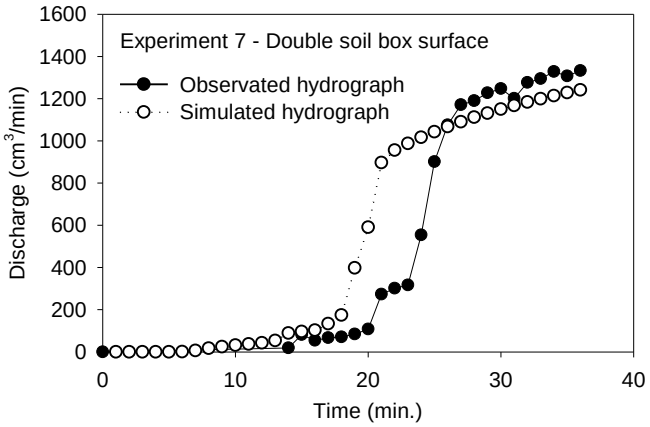

Figure 3.17. Comparison of the observed and simulated hydrographs for Experiment 7, using a silty clay loam.

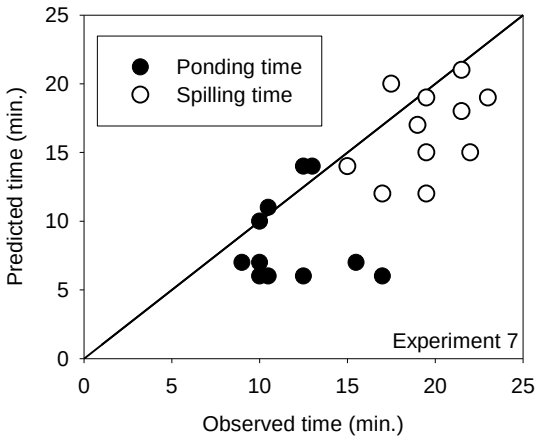

Figure 3.18. Comparison of the simulated and observed critical times of puddle filling and spilling processes for Experiment 7 using a silty clay loam.

Fig. 3.19 and Table 3.8 display the average modeled and observed wetting front depths and the quantitative evaluation of model performance. The relatively high EF and low NOF values (Table 3.8) indicate that the model simulations are in good agreement with the observed results.

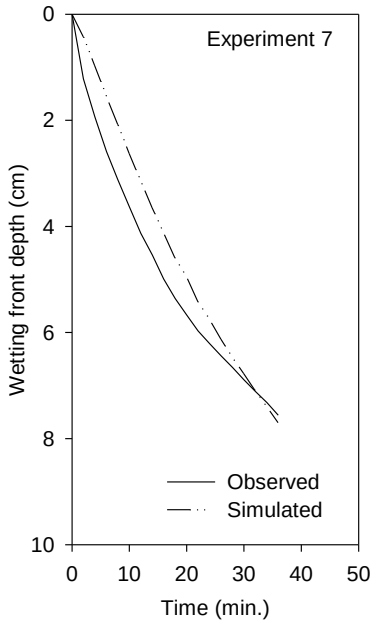

Figure 3.19. Comparison of the simulated and observed average wetting front depths for Experiment 7 using a silty clay loam.

Table 3.8. Normalized Objective Function (NOF) and Modeling Efficiency (EF) of the Observed and Simulated Average Wetting Front Depths for Experiment 7

Experiment 7	EF	0.90
	NOF	0.16

3.4. Summary and Conclusions

A series of experiments focusing on the effects of microtopography on overland flow generation were conducted in the Overland Flow Laboratory. These experiments considered two types of surfaces that differed in microtopography. All other conditions of the individual experiment were identical between the surfaces (e.g., soil type, rainfall, and initial moisture content). Additionally, the P2P model was employed to simulate the physical processes and compare against the observed results. The experiments generally

showed that during the first rainfall event, the rough surface had an equivalent or lower steady state flow after full connectivity was achieved. The equivalent steady state flow combined with a delayed initial discharge from the rough surface generally caused a lower runoff volume during initial rainfall events. This trend was true across soil types and also the range in initial soil moisture contents. Interestingly though, given complex rainfall conditions, the rough surface experienced greater runoff generation in subsequent rainfalls. Over the course of several rainfall events, the rough surface overtook the smooth surface in steady state flows after full connectivity was achieved. To a lower extent, the runoff generation capacity of the rough surface had increased beyond the capacity of the smooth surface even during an unsteady rain event of a long duration. It should be noted that this shift in runoff generation inequality came after the rainfall intensity had dropped so low that a non-ponding stage was induced and then the intensity was switched back to a sufficient level to generate surface runoff.

The results of a set of laboratory experiments were compared with the simulations by the P2P model. In most cases, the results from the P2P model were found to be in good agreement with the observed data of the experiments. The results that were compared between the simulated and observed data included the hydrographs, ponding times, spilling times, and wetting front depths. The tested factors varied across soil type, rainfall pattern (including unsteady and complex patterns), and initial soil moisture content. The P2P model has been shown capable of simulating the physical processes observed in the experiments and achieving good agreements with the observed data.

CHAPTER 4. OVERALL CONCLUSIONS AND FUTURE RESEARCH

This thesis examined the effects of surface microtopography on runoff generation. Specific factors of hydrology considered in conjunction with microtopography ranged from soil type and initial moisture content to rainfall intensity and patterns (including natural rainfall). Additionally, the Windows-based P2P modeling software was found to be well suited to studies in microtopography-controlled overland flow and the simulation results were compared with the experimental data. The model was capable of characterizing complex microtopographic surfaces and simulating overland flow and unsaturated flow under various hydrologic conditions.

Specifically, Chapter 2 presented a field study that took place during the summer of 2011. During that time period, two natural rainfall events were intercepted and hydrologic processes under the influence of microphotography were observed and recorded. Additionally, surface information was quantified in an attempt to link its microtopographic characteristics to the surface runoff generation for both events. It appeared that the runoff generational characteristics of the rough surface changed between the events while the smooth surface runoff generation did not differ greatly. During the second rainfall event, runoff generation did not dramatically decrease as a ratio to total rainfall for the rough surface, despite a much lighter intensity rainfall which should have induced more infiltration. Conversely, the smooth surface did exhibit a marked difference in the ratio of runoff to total rainfall input. These observations led to the conclusion that surface roughness had a temporal effect on the infiltration characteristics of a surface.

In Chapter 3, a more in-depth look over an array of laboratory experiments over several hydrologic variables was undertaken. Factors such as soil type, initial moisture

content, and rainfall patterns were considered. These experiments took place in a controlled laboratory environment. The results of these experiments were compared against the outputs of the P2P model for various rainfall events, soil types, and initial moisture conditions of the physical experiments.

Through physical experimentation, a general trend was observed for initial rainfall events: the rougher surface contributed an equal or lower runoff rate than its smoother counterpart. However, during subsequent events runoff generational output from the rough surface showed a marked increase in comparison with the smooth surface. Indeed, the rough surface runoff generation subsequently overtook the smooth surface in an experiment that considered multiple rainfall events. These observations were in alignment with the conclusions of the field study. Good agreement was found between the observed data of the physical laboratory experiments and the P2P model simulations. On the whole, the P2P model was capable of handling a complex set of soil, surface microtopography, and rainfall events.

With regard to future research, more physical experimentation with a focus on multiple rainfall events over rough and smooth surfaces is imperative. It has been recently demonstrated (Fox 1998) that microtopography increases surface sealing at puddle centers. The degree in which this process takes place should be studied in conjunction with the aforementioned hydrologic factors of this thesis (i.e., soil type, initial moisture content, rainfall intensity). For example, recreating a set of physical laboratory experiments similar to the ones performed in this research focusing on complex rainfall events. Doing such would provide more insight into how different conditions (e.g., soil type and initial moisture content) affect temporal changes in soil infiltrability. Additional physical experimentation

would be to cross-examine all conditions against others. As an example, a set of experiments can be executed, in which both coarse and fine soil types are tested at various initial moisture contents using both rough and smooth surfaces. Such a cross examination of these conditions would provide complete array of the effects of these factors in conjunction with microtopography. A greater understanding of the related hydrologic processes certainly holds value for future modeling work that should be done in this area.

LITERATURE CITED

ASTM, 2003 Standard Test Methods for Laboratory Determination of Water (Moisture) Content of Soil and Rock by Mass, ASTM D2216-10, Philadelphia.

Blanquies, J., Scharff, M., and Hallock, B., 2003 The design and construction of a rainfall simulator. *IECA*, 34th Conf., Las Vegas, NV., Feb., 24-28.

Bouwer, H., "Rapid field measurement of air-entry value and hydraulic conductivity of soil as significant parameters in flow system analysis." *Water Resour. Res.*, 2(4), 729-739.

Burwell, R.E, and Larson, W.E., 1969 Infiltration as influenced by tillage-induce random roughness. *Soil Sci. Soc. Am. J.* 33(3). 449-452.

Chu, X., 2011 Characterization of Microtopography and its Hydrologic Significance, Chapter 1, p1-14. In: *Modeling Hydrologic Effects of Microtopographic Features* (ISBN 978-1-61668-628-4), edited by X. Wang. Nova Science Publishers, Inc.

Chu, X., and Mariño, M.A., 2005 Determination of ponding condition and infiltration into layered soils under unsteady rainfall. *J. Hydrol.*, 313(3-4), 195-207.

Chu, X., Yang, J., Chi, Y., and Zhang, J., 2013. Dynamic puddle delineation and modeling of puddle-to-puddle filling-spilling-merging-splitting overland flow processes. *Water Resour. Res.*, 49(6), 3825-3829.

Chu, X., Zhang, J., Chi, Y., and Yang, J., 2010a An improved method for watershed delineation and computation of surface depression storage. Proc., Watershed Management 2010: *Innovations in Watershed Management Under Land Use and Climate Change, ASCE*, WI., 1113-1122.

Chu, X., Zhang, J., Yang, J., and Chi, Y., 2010b Quantitative evaluation of the relationship between grid spacing of DEMS and the surface depression storage. Proc., World

Environmental and Water Resources Congress 2010: *Challenges of Change, ASCE*, RI., 4447-4457.

Chu, X., Zhang, J., Yang, J., Chi, Y., Yang, Y., and Habtezion, N., 2013 *Scanned Data Combination – S-C Tool, User's Manual*. North Dakota State University.

Cogo, N.P., Moldenhauer, W.C., and Foster, G.R., 1983 Effect of crop residue, tillage-induced roughness, and runoff velocity on size distribution of eroded soil aggregates. *Soil Sci. Soc. Am. J.* 49(5), 1005-1008.

Cogo, N.P., Moldenhauer, W.C., and Foster, G.R., 1984 Soil loss reductions from conservation tillage practices. *Soil Sci. Soc. Am. J.* 48(2), 368-373.

Darboux, F., Davy, Ph., Gascuel-Odoux, C., and Huang, C., 2001 Evolution of soil roughness and flowpath connectivity in overland flow experiments. *Catena* 46(2/3), 125-139.

Darboux, F., Davy, P., and Gascuel-Odoux, C., 2002 Effect of depression storage capacity on overland flow generation for rough horizontal surfaces: Water transfer distance and scaling. *Earth Surf. Proc. Land.* 27(2), 177-191.

Darboux, F., and Huang, C., 2003 An instantaneous-profile laser scanner to measure soil surface microtopography. *Soil Sci. Soc. Am. J.* 67(1), 92-99.

Darboux, F., and Huang, C., 2005 Does soil surface roughness increase or decrease water and particle transfers? *Soil Sci. Soc. Am. J.* 69(3), 748-756.

Diskin M.H., and Nazimov, N., 1996 Ponding time and infiltration capacity variation during steady rainfall. *J. Hydrol.* 178(1), 369-380.

Favis-Mortlock, D., 1998 A self-organizing dynamic systems approach to the simulation of rill initiation and development on hillslopes. *Comp. Geosci.* 24(4), 353–372.

Fox, D.M., Le Bissonnais, Y., and Bruand, A., 1998a The effect of ponding depth on infiltration in a crusted surface depression. *Catena* 32(2), 87-100.

Fox, D.M., Le Bissonnais, Y., and Quétin, P. 1998b The implications of spatial variability in surface seal hydraulic resistance for infiltration in a mound and depression microtopography. *Catena* 32(2), 101-114.

Gomez, J.A., and Nearing, M.A., 2005 Runoff and sediment losses from rough and smooth soil surfaces in a laboratory experiment. *Catena* 59(3), 253-266.

Helming, K., Römkens, M.J.M, and Prasad, S.N., 1998 Surface roughness related process of runoff and soil loss: A flume study. *Soil Sci. Soc. Am. J.* 62(1), 243-250.

Huang, C., and Bradford, J.M., 1990 Portable laser scanner for measuring soil surface roughness. *Soil Sci. Soc. of Am. J.* 54(5), 1402-1406.

Ibbit, R.P., and O'Donnell, T., 1971 Fitting methods for conceptual catchment methods. *J. Hydraul. Div.* 97(9), 1331 - 1342

Jackson, T.J., and Schmugge, T. J. 1989 Passive microwave remote sensing system for soil moisture: Some supporting research. *IEEE Trans. Geosci. Remote Sens.* GE-27, 225-235.

Johnson, C.B., Mannering, J.V., and Moldenhauer W.C., 1979 Influence of surface roughness and clod size stability on soil and water losses. *Soil Sci. Soc. Am. J.* 43(4), 772-777.

Meyer, L. D. 1994 Rainfall simulators for soil erosion research. In: *Soil Erosion Research Methods*, 2nd Edition, edited by R. Lal. CRC Press.

Meyer, L.D., and Harmon, W. C. 1979 Multiple-intensity rainfall simulator for erosion research on row sideslopes. *Trans. ASAE*, 22, 100-103.

Moldenhauer, W.C., 1970 Influence of rainfall energy on soil loss and infiltration rates: II. Effect of clod size distribution. *Soil Sci. Soc. Proc.* 34(4), 673-677.

Moore, I.D., and Larson, C.L., 1979 Estimating micro-relief surface storage from point data. *Trans. ASAE.* 22(5), 1073-1077.

Nash, J.E., and Sutcliffe, J.V., 1970 River flow forecasting through conceptual models, Part 1: A discussion of principles. *J. Hydrol.* 10(3), 282-290.

O'Callaghan, J. F., and Mark, D. M. 1984 The extraction of drainage networks from digital elevation data. *Comp. Vision, Graphics, and Image Proc.* 28(3), 323-344.

Onset Computer Corp., 2005 Data Logging Rain Gauge RG3 and RG3-M User's Manual.

Onstad, C.A., 1984 Depressional storage on tilled soil surfaces. *Trans. ASAE* 27(3), 729-732.

Rawls, W.J., and Brakensiek, D.L. 1983 Green and Ampt infiltration parameters from soil data. *J. Hydraul. Eng.,* 109(1), 62–70.

Römkens, M.J.M., and Wang, J.Y., 1986 Effect of tillage on surface roughness. *Trans. ASAE* 29(2), 429-433.

Sande, L., Chu, X., and Desutter, T. 2011 A new method for replicating complex microtopographic surfaces in laboratory soil box experiments. *App. Environ. Soil Sci.*, 27(4), 615-620.

Schaap, M.G., Leij, F.J., and van Genuchten, M.T., 2001 Rosetta: A computer program for estimating soil hydraulic parameters with hierarchical pedotransfer functions. *J. Hydrol.* 251, 163-176.

Smith, R.E., 1972 The infiltration envelope: Results from a theoretical infiltrometer.

J. Hydrol. 17(1), 1-22.

Soil Survey Staff, Natural Resources Conservation Service, United States Department of Agriculture. (2013) Web Soil Survey. <*http://websoilsurvey.nrcs.usda.gov*> Accessed November 1, 2013

Van Genuchten, M.T., 1980 A closed form equation for predicting the hydraulic conductivity of unsaturated soils. *Soil Sci. Soc. Am. J.,* 44(5), 892-898.

Yang, J., and Chu, X. 2013a Effects of DEM resolution on surface depression properties and hydrologic connectivity. *J. Hydrol. Eng.*, 18(9) 1157-1169.

Yang, J., and Chu, X., 2013b Quantification of the spatio-temporal variations in hydrologic connectivity of small-scale topographic surfaces under various rainfall conditions. *J. Hydrol.* 505:65-77.